The Astrophysical Journal, 892:98 (15pp), 2020 April 1 https://doi.org/10.3847/1538-4357/ab7cde

Spatial Distribution of Electromagnetic Waves near the Proton Cyclotron Frequency in ICME Sheath Regions Associated with Quasi-perpendicular Shocks: Wind Observations

Q. H. Li[1,2], L. Yang[1,3], L. Xiang[4], and D. J. Wu[1]
[1] Key Laboratory of Planetary Sciences, Purple Mountain Observatory, CAS, Nanjing 210034, People's Republic of China; ylei@pmo.ac.cn
[2] School of Astronomy and Space Science, University of Science and Technology of China, Hefei 230026, People's Republic of China
[3] State Key Laboratory of Space Weather, National Space Science Center, CAS, Beijing 100190, People's Republic of China
[4] Key Laboratory of Low Dimensional Quantum Structures and Quantum Control, Hunan Normal University, 410081, Changsha, People's Republic of China
Received 2020 January 16; revised 2020 March 2; accepted 2020 March 3; published 2020 April 2

Abstract

Electromagnetic waves (EMWs) near the proton cyclotron frequency f_{cp} are transverse left-handed (LH) or right-handed (RH) polarized waves, and are ubiquitous in the solar wind. However, the characteristics of these waves in the sheath regions of interplanetary coronal mass ejections (ICMEs) are poorly understood. Through a comprehensive survey of Wind magnetic field and plasma data using dynamic spectra and repeated filtering analyses, 700 EMW events (7.1% of the analysis time) are identified in the 62 ICME sheath regions associated with quasi-perpendicular shocks involved with a low shock Mach number M_f and low upstream β_1. In the ICME sheath regions, outward (inward)-propagating LH (RH) EMWs have relatively higher counts and longer duration than inward (outward)-propagating LH (RH) EMWs in the plasma frame, consistent with previous STEREO observations. The spatial distributions of the magnetic field, plasma, and frequency parameters of EMWs are also presented in both spacecraft and plasma frames, especially the proton (alpha) temperature anisotropy $T_{p(\alpha)\perp}/T_{p(\alpha)\parallel}$, α abundance N_α/N_p, and normalized differential alpha-proton speed V_d/V_A. After removing the Doppler shift, 81.1% (59%) of all outward (inward)-propagating LH EMWs have a frequency below (above) $0.5f_{cp}$, while 68.3% (64%) of all outward (inward)-propagating RH EMWs have a frequency smaller (greater) than $0.5f_{cp}$. Further investigations of local plasma parameters reveal that different excitation mechanisms for EMWs are in different subregions of the ICME sheath regions. These results are helpful in understanding the important role of EMWs in the solar wind–ICME coupling process with different sheath regions.

Unified Astronomy Thesaurus concepts: Interplanetary magnetic fields (824); Solar coronal mass ejection shocks (1997); Solar wind (1534); Space plasmas (1544)

1. Introduction

As one of the active research areas in solar winds, electromagnetic waves (EMWs) near the ion cyclotron frequency play an important role in the dynamics of various plasma environments (Ofman et al. 2002; Russell & Blancocano 2007; Araneda et al. 2008; Kasper et al. 2013; Omidi et al. 2014; Remya et al. 2014; Allen et al. 2015; Gary et al. 2016). These waves are left-hand (LH) or right-hand (RH) circularly polarized for parallel propagation and are elliptically polarized for oblique propagation (Stix 1962; Gary 1993; Omidi et al. 2011). In the case of parallel propagation, the maximum variance direction $\boldsymbol{i}$ of the EMW magnetic fields is almost perpendicular to the $\boldsymbol{B}_0$–$\boldsymbol{k}$ plane (where $\boldsymbol{k}$ and $\boldsymbol{B}_0$ are the wavevector and the background magnetic field, respectively) for LH polarization (i.e., Alfvén-cyclotron waves; Gary 1993), but is nearly parallel to the $\boldsymbol{B}_0$–$\boldsymbol{k}$ plane for RH polarization (i.e., magnetosonic/whistler waves; Gary 1993). EMWs have been observed in the inner heliosphere from 0.3 to 1 au and statistically studied to determine their excitation mechanisms and related wave–particle interaction processes (Tsurutani et al. 1994; Jian et al. 2009, 2010; Boardsen et al. 2015; Zhao et al. 2019). Besides, observations also present evidence of the absorption of EMW energy at the proton cyclotron frequency, responsible for the energy conversion therein (Denskat et al. 1983; Gary et al. 2001; Hamilton et al. 2008). Owing to the important role of EMWs in the solar wind and geomagnetic environments, it is necessary to understand when, where, and under what conditions EMWs can grow or not.

Ion temperature anisotropy is widely accepted as one of the main excitation mechanisms for EMWs and often has two branches: ion cyclotron anisotropy instability and parallel firehose instability (Kasper 2002; Hellinger et al. 2006; Bale et al. 2009; Maruca et al. 2012; Bourouaine et al. 2013; Yoon 2017). The ion cyclotron anisotropy instability grows fast at $\boldsymbol{k}\|\boldsymbol{B}_0$ when the perpendicular ion temperature $T_{i\perp}$ is greater than the parallel ion temperature $T_{i\parallel}$ in a low-β plasma (Price et al. 1986; Gary 1993; Lu & Wang 2006; Yoon 2017), but when $T_{i\parallel} > T_{i\perp}$ in a high-β plasma, the parallel firehose instability grows fast and excites magnetosonic/whistler waves (Gary 1993; Hellinger et al. 2006; Yoon 2017). These two types of instabilities then regulate the solar wind ion distribution functions. Another main excitation mechanism for EMWs is ion beams that can provide free energy for the excitation process (Russell & Blancocano 2007; Araneda et al. 2008; Ofman et al. 2017; Klein et al. 2018; Xiang et al. 2018a, 2018b). For a ring or ring-beam distribution perpendicular to the background magnetic field, ion cyclotron waves will grow through the ion cyclotron ring instability (Simons et al. 1980; Convery & Gary 1997; Leamon et al. 2000; Hamilton et al. 2008). The RH magnetosonic/whistler waves will grow faster through the ion beam instability, which is comparatively isotropic and cool (Simons et al. 1980; Tsurutani & Smith 1984; Convery & Gary 1997; Leamon et al. 2000; Hamilton et al. 2008).

Coronal mass ejections (CMEs) are major solar transient events occurring in the solar atmosphere (e.g., Howard et al. 1985; Crooker et al. 1997; Forbes 2000; Low 2001; Webb & Howard 2012). The ejecta of CMEs in the solar wind, as a key

link between solar activities and disturbances in the heliosphere, are now referred to as interplanetary coronal mass ejections (ICMEs; Burlaga et al. 1982; Richardson & Cane 2004; Zurbuchen & Richardson 2006; Howard & Tappin 2009). They are generally described as flux-rope-like structures which are believed to be magnetically connected to the Sun during their outward propagation in the solar wind (e.g., Burlaga 1988; Russell et al. 1990; Howard & Tappin 2009). For an ICME associated with an interplanetary fast shock, a sheath region is formed between this shock front and the leading edge of the ICME (Russell & Mulligan 2002; Huttunen & Koskinen 2004; Kataoka et al. 2005; Kaymaz & Siscoe 2006; Siscoe & Odstrcil 2008). Due to both the CMEs' propagation relative to the solar wind and its expansion (e.g., Kaymaz & Siscoe 2006; Siscoe & Odstrcil 2008; Good et al. 2015), the ICME sheath regions are compressed, hot, and turbulent solar wind plasmas. They can accumulate gradually over long time periods and keep the evolutionary history of the interaction with the solar wind over a range of heliocentric distances (Crooker & Horbury 2006; Kaymaz & Siscoe 2006; Siscoe & Odstrcil 2008; Richardson & Cane 2011; Kilpua et al. 2017). Generally, compared with the ICME proper, the sheath regions are more turbulent, associated with more anisotropic ion temperatures, much larger plasma β due to higher plasma pressure, denser plasmas, higher dynamic pressure, and larger Alfvén Mach numbers (Crooker & Siscoe 1977; Guo et al. 2011; Yermolaev et al. 2012; Myllys et al. 2016). These properties are of paramount importance for studies on not only the solar wind–ICME coupling process (Kaymaz & Siscoe 2006; Richardson & Cane 2011; Kilpua et al. 2017) but also the present space weather due to possible roles of ICME sheaths in driving intense geomagnetic storms (Tsurutani et al. 1988; Richardson et al. 2001; Huttunen et al. 2002; Huttunen & Koskinen 2004; Kilpua et al. 2017), impeding the propagation of energetic particles (Sanderson et al. 2000; Klecker et al. 2006; Russell et al. 2013), and showing the geometries of oncoming ICMEs (Jones et al. 2002). However, relatively little is known about the distributions of the magnetic field and plasma fluctuations within these sheath regions. It is a challenging task to predict the fine structure of the sheath regions because of the turbulent nature of the magnetic field and plasma variations here (Bale et al. 2005; Burgess et al. 2005; Kilpua et al. 2013, 2017; Moissard et al. 2019).

Due to the very different structure, dynamics, and dissipation processes of the interplanetary shock (depending on not only the shock angle θ_{Bn} between the shock normal and the upstream magnetic field, but also the upstream plasma beta β_1, i.e., the ratio of plasma to magnetic pressure), the ICME sheath regions can be usually divided into two categories: the quasi-parallel sheath regions located downstream of quasi-parallel shocks ($\theta_{Bn} < 45^\circ$) and the quasi-perpendicular sheath regions where $\theta_{Bn} > 45^\circ$ (Cane 1988; Bale et al. 2005; Manchester et al. 2005; Janvier et al. 2014; Zank et al. 2015). Both the quasi-parallel and the the quasi-perpendicular ICME sheath regions are all turbulent, especially the former, which frequently exhibit strong turbulence and can lead to rapid acceleration at interplanetary shocks (Burgess et al. 2005; Zank et al. 2015). For a quasi-parallel shock, upstream ions are reflected by the shock front and can move far upstream along the magnetic field, exciting low-frequency plasma waves through the plasma beam instability (Quest et al. 1983; Omidi et al. 1990; Krauss-Varban & Omidi 1991; Kuramitsu & Krasnoselskikh 2005; Hao et al. 2016). But for quasi-perpendicular shocks, the reflected ions, on the contrary, gyrate back to the shock and enter the downstream region, in which the magnetic fluctuation level is substantially higher than the upstream (Lee et al. 1988; Wilkinson 1995; McKean et al. 1995; Lu & Wang 2006; Ofman et al. 2009; Wilson et al. 2009; Hao et al. 2014). As a result, these reflected ions are energized in the perpendicular direction, and then have ion temperature anisotropy ($T_{i\perp} > T_{i\parallel}$) near the shock front (Lee et al. 1988; McKean et al. 1995; Lembege et al. 2004). Both theoretical and simulation works have shown that such a temperature anisotropy is unstable for ion cyclotron waves and mirror waves (Gary et al. 1976, 1994; McKean et al. 1996; Gary et al. 2003; Lu & Wang 2006; Hao et al. 2014), and in the downstream of the quasi-perpendicular shocks, observational evidence has been found for the ion cyclotron waves in a low-β plasma and mirror waves in a high-β plasma (Anderson et al. 1991; Anderson & Fuselier 1993; Song et al. 1994).

When spacecraft pass an interplanetary shock to the inner ICME, large-amplitude and turbulence-like electromagnetic field fluctuations are often observed in the ICME sheath region (Kataoka et al. 2005; Liu et al. 2006; Russell et al. 2009; Kajdič et al. 2012; Kilpua et al. 2013; Ala-Lahti et al. 2019; Moissard et al. 2019). These fluctuations can be classified into some wave modes by analyzing the magnetic field and plasma data. The characteristics and dynamics of EMWs could be affected by the nonuniform and turbulent sheath regions of ICMEs. Due to their important role in the heating and acceleration of ion particles (especially minor heavy ions, e.g., alpha particles; Marsch et al. 1982; Bourouaine et al. 2011, 2013; Maruca et al. 2012; Verscharen et al. 2013; Maneva et al. 2015), the excitation mechanisms of EMWs in ICME sheaths are still not clear. Although EMWs have been statistically examined in ICME sheath regions from STEREO observations (Li et al. 2019), there are no detailed information on the plasma parameters, especially the temperature anisotropy and alpha particles, which can be used to determine the mechanism for exciting EMWs there. The dependence of these wave characteristics on shock properties is also not clear.

In the sheath regions, the free energy sources for exciting these waves are expected to be kinetic-scale or fluid-like processes at the ICME-driven shock, within the sheath region, and at the leading edge of ICMEs. Due to the inhomogeneity and the variations of the background plasma/magnetic field in the ICME sheath regions, it becomes more difficult to understand the excitation mechanism of these EMWs. To overcome these problems, Wind data will be used in the present work to further study the spatial distributions and statistical properties of EMWs in ICME sheath regions associated with interplanetary shocks. In the present paper, considering stronger turbulence of the sheath regions behind quasi-parallel shocks, only the ICME sheath events with quasi-perpendicular shocks are selected, and those events with quasi-parallel shocks will be left to a future work. Our results may be helpful in understanding the microphysical process of EMW–particle and the solar wind–ICME interactions when the locations of EMWs in the sheath region and conditions favorable for exciting these waves are known.

The rest of the present paper is organized as follows. Three typical ICME sheath regions associated with EMWs are presented and analyzed in detail in Section 2, and the relevant statistical analyses in both spacecraft and plasma frames are provided in Section 3 to illustrate the spatial distribution characteristics of

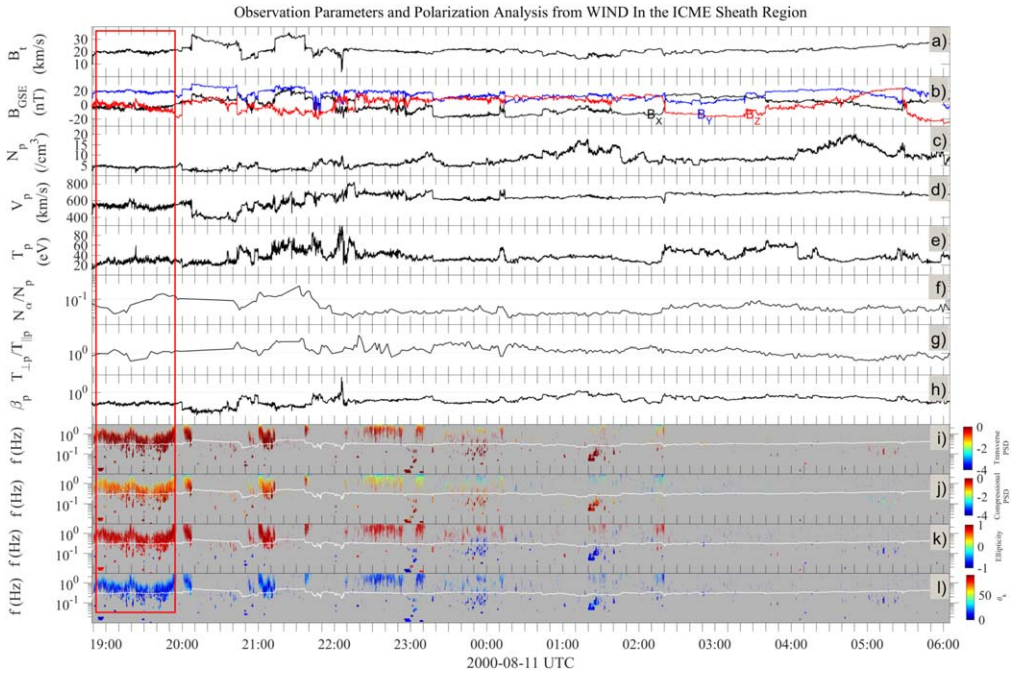

Figure 1. Observations of the sheath region of an ICME on 2000 August 11–12. (a) Total magnetic magnitude ($|B|$), (b) magnetic field components B_X, B_Y, and B_Z in GSE coordinates, (c) proton density N_p), (d) proton velocity V_p, (e) proton temperature T_p, (f) α abundance N_α/N_p, (g) proton temperature anisotropy $T_{p\perp}/T_{p\|}$, (h) proton beta β_p, (i) the power spectral density (PSD) of the transverse magnetic field, (j) the compressional magnetic PSD, (k) the ellipticity in the spacecraft frame, where the positive (negative) sign corresponds to RH (LH) circular polarization, and (l) the propagation angle $\theta_{\boldsymbol{kB}_0}$. Gray regions correspond to the signal with both DOP (the degree of polarization) and $|\epsilon|$ below 0.7. White traces in (i)–(l) indicate the local proton gyrofrequency.

EMWs in the sheath regions associated with quasi-perpendicular shocks. Section 4 is devoted to related discussions about the statistical results in Section 3, and in the final section, the main results of the present work are summarized.

2. Case Analysis

To study EMWs in the ICME sheath region, we use the 0.092 s and 3 s magnetic field from the Wind MFI instrument (Lepping et al. 1995), the 3 s plasma data from the Wind 3DP instrument (Lin et al. 1995), and the 92 s solar wind alpha and proton anisotropy parameters from the Wind SWE instrument (Ogilvie et al. 1995; Kasper et al. 2006). Based on the criteria for identifying EMWs mentioned by Jian et al. (2009, 2010), we combine the minimum variance analysis (MVA) with the repeated filtering analysis methods to analyze the polarization properties of EMWs in the plasma frame (Li et al. 2019). In this section, we will present three typical ICME sheath regions with EMWs near the quasi-perpendicular leading shock, within the middle sheath region, and near the ICME leading edge.

2.1. EMWs near a Quasi-perpendicular Leading Shock

Figure 1 shows an example of an ICME sheath region observed by the Wind spacecraft during 2000 August 11 18:49 UT (the leading shock time) and 2000 August 12 06:05 UT (the leading edge of the ICME). For the leading shock, the shock angle θ_{Bn} is 78°.2, Alfvén Mach number is 2.267, fast magnetoacoustic Mach number is 1.27, and the upstream plasma beta β_1 (the ratio of thermal to magnetic pressure) is 0.032. From these shock parameters, it is clear that the succeeding ICME drives a fast and quasi-perpendicular shock. Panels (a)–(h) of Figure 1 show the magnetic field and plasma parameters in the sheath region. The magnetic dynamic spectra of the ICME sheath region in the spacecraft frame are shown in Figures 1(i)–(l), where the local proton gyrofrequency is represented by the white trace. Correspondingly, the gray regions in Figures 1(i)–(l) correspond to the signal with both the degree of polarization and $|\epsilon|$ below 0.7.

In this sheath region, we found a total of 26 EMW events, each with duration longer than one minute. The total duration of these EMWs is 225.58 minutes, accounting for 33.37% of the whole sheath region (lasting 676 minutes). Dynamic spectral analysis (see Figures 1(i)–(l)) of the magnetic field shows that most EMWs occur in the front part of the sheath region, especially near the downstream of the leading shock. The plasma in this region has the following characteristics: violent magnetic disturbances of each component in the GSE coordinate system (see Figure 1(b)), enhanced magnetic field intensity and velocity variations (Figures 1(a) and (d), respectively), and high α abundance N_α/N_p (Figure 1(f)). In the whole sheath region, the proton beta is not very high (lower than one, in Figure 1(h)), and the proton temperature anisotropy $T_{p\perp}/T_{p\|}$ is generally higher than 1 (the mean value of $T_{p\perp}/T_{p\|}$ is 1.716, see Figure 1(g)).

To understand the physical characteristics of these waves, we performed a further wave analysis for each wave event in the whole sheath region. Figure 2 shows an example of an inward-propagating LH EMW near the downstream of the leading quasi-perpendicular shock, corresponding to the region marked by the red box in Figure 1. The time duration for this wave event is 63.67 minutes (18:51:00–19:54:40 on 2000 August 11). As can be seen from Figure 1(k), these EMWs are RH polarized in the spacecraft frame. By repeated filtering analysis, we can obtain the frequency range of $f_{min} = 0.148$ Hz to $f_{max} = 1.8$ Hz for these waves and the corresponding bandwidth $\Delta f_{sc} = 1.652$ Hz in the spacecraft frame. Figures 2(a)–(d) show the background magnetic field in

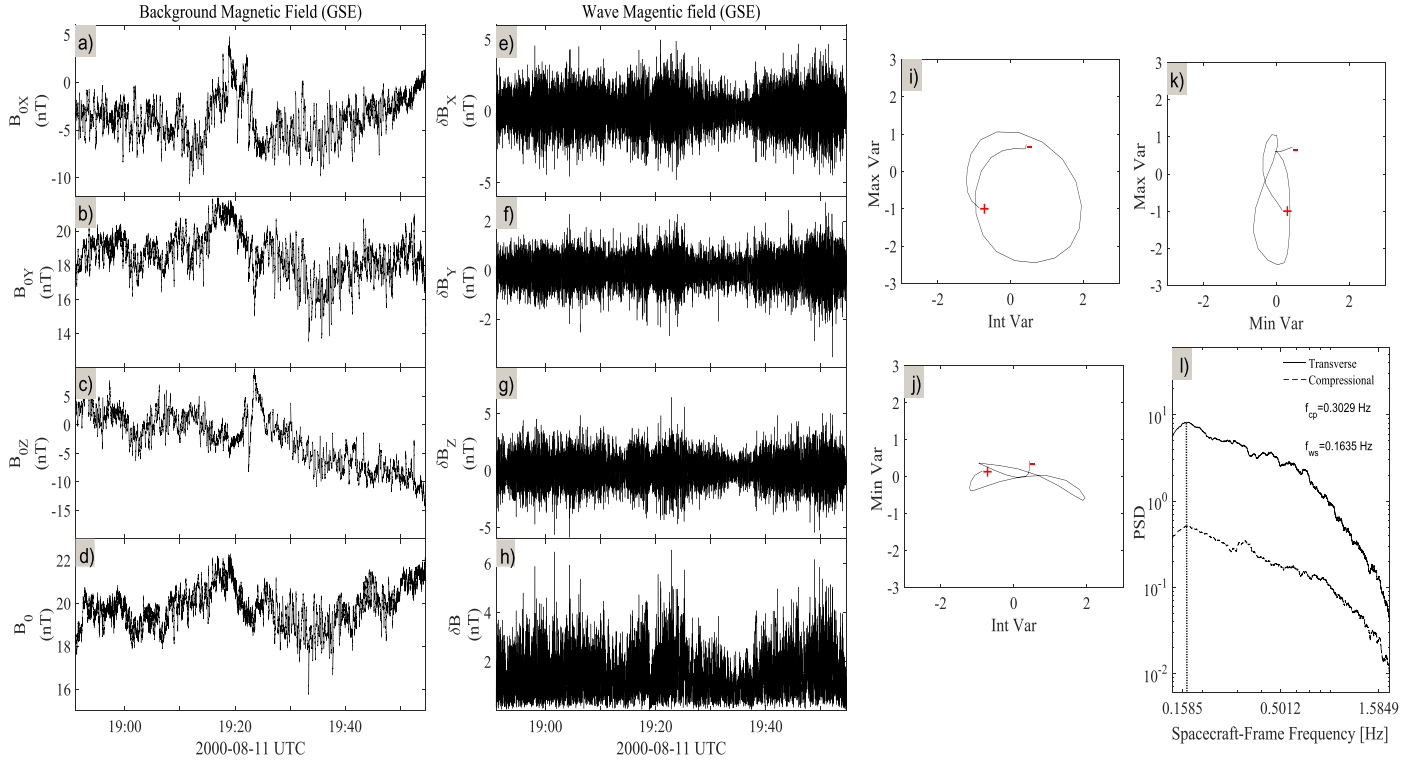

Figure 2. Characteristics of inward-propagating LH EMWs near a quasi-perpendicular leading shock (i.e., the region marked by the red box in Figure 1). (a)–(d) The background magnetic field in GSE coordinates, (e)–(h) the wave field in GSE coordinates, (i)–(k) hodograms of the wave magnetic field from MVA, and (l) the power spectral densities of the transverse and compressional magnetic fluctuations. The beginning and the ending of wave cycles are marked with + and −, respectively. In Figure 2(i), $\boldsymbol{B}_0$ points into the paper.

GSE coordinate system, and the related wave field $\delta\boldsymbol{B}$ between $f_{\rm min}$ and $f_{\rm max}$ in the same coordinate system is shown in Figures 2(e)–(h). We performed the MVA for the wave field. As a result, the angle $\theta_{\boldsymbol{kB}_0}$ between the background magnetic field $\boldsymbol{B}_0$ and the minimum variance direction $\boldsymbol{k}$ is 3°.19. A short time of the hodogram of the wave field $\delta\boldsymbol{B}$ in the MVA coordinate system is shown in Figures 2(i)–(k). It can be seen from Figure 2(i) that these waves are RH polarized in the spacecraft frame with $\boldsymbol{B}_0$ pointing into the paper. The ratio $\lambda_{\rm int}/\lambda_{\rm min}$ between the intermediate and minimum eigenvalues is 5.02, indicating that these waves are plane waves.

Based on the directions of $\boldsymbol{k}$ and $\boldsymbol{B}_0$, we introduce the SAK orthogonal coordinate system. In such a plasma frame, $\boldsymbol{A}$ ($=\boldsymbol{k}\times\boldsymbol{\mathcal{B}}_0/|\boldsymbol{k}\times\boldsymbol{\mathcal{B}}_0|$) is perpendicular to the $\boldsymbol{B}_0$–$\boldsymbol{k}$ plane, and $\boldsymbol{S}$ ($=\boldsymbol{A}\times\boldsymbol{k}$) is parallel to the $\boldsymbol{B}_0$–$\boldsymbol{k}$ plane (Stix 1962; Blanco-Cano & Schwartz 1995). In this way, the observed angle θ_{Ai} between $\boldsymbol{A}$ and the maximum variance direction $\boldsymbol{i}$ is 19°.6, indicating that the maximum variance direction of the wave field is nearly perpendicular to the $\boldsymbol{B}_0$–$\boldsymbol{k}$ plane. The characteristics of these waves are consistent with LH-polarized EMWs in the plasma frame. The wave polarization reversal from the spacecraft to plasma frames indicates that these waves are inward-propagating LH EMWs in the plasma frame. That is to say, the LH EMWs travel away from the leading shock and toward the middle sheath region. The spectral analysis of transverse and compressional magnetic fluctuations is shown in Figure 2(l), and there is one peak frequency for this wave event in the spacecraft frame, i.e., $f_{\rm ws}=0.1635$ Hz (indicated by the vertical dotted line). After removing the Doppler effect of the solar wind flow given by Jian et al. (2009), the wave peak frequency in the plasma frame is $f_{\rm wp}\approx 0.2454$ Hz, below the local proton cyclotron frequency $f_{\rm cp}=0.3029$ Hz.

On the other hand, the mean value of $T_{\rm p\perp}/T_{\rm p\parallel}$ is 1.0016, i.e., the proton temperature is almost isotropic, implying that these EMWs may not be excited by the local proton temperature anisotropy instability. The mean value of $T_{\alpha\perp}/T_{\alpha\parallel}$ is 0.637, implying that the local alpha temperature anisotropy instability may not excite these inward-propagating LH EMWs. However, we cannot rule out that these inward-propagating LH EMWs have been excited through ion temperature anisotropy instability by the time the local plasma is near quasilinear saturation state during the measurements. Furthermore, the normalized differential alpha-proton speed $V_{\rm d}/V_{\rm A}$ is 0.282 in units of the Alfvén speed $V_{\rm A}$. The α abundance $N_\alpha/N_{\rm p}$ for this event is 6.67%, higher than that in a typical solar wind (usually 4%).

2.2. EMWs within a Middle Sheath Region

Figure 3 shows an example of an ICME sheath region observed by the Wind spacecraft on 2002 April 19–20. The leading shock is at 08:24 UT on 2002 April 19, and the leading edge of ICME is at 06:57 UT on 2002 April 20. In this ICME event, the leading shock angle θ_{Bn} is 80°.12, the Alfvén Mach number is 2.488, the fast magnetosonic Mach number is 1.12, and the upstream plasma beta β_1 is 1.085. It can be seen that the leading shock is a fast and quasi-perpendicular shock. In the sheath region, we found a total of 16 EMW events. The total duration of these EMWs is 71.583 minutes, accounting for 5.29% of the whole sheath region (∼1353 minutes). Dynamic spectral analysis (see panels (i)–(l) of Figure 3) shows that most EMWs occur in the middle sheath region with frequencies higher than the local proton cyclotron frequency. In the whole sheath region, the mean value of proton beta is 0.7 (Figure 3(h)), the α abundance $N_\alpha/N_{\rm p}$ (its mean value is nearly 10%; see

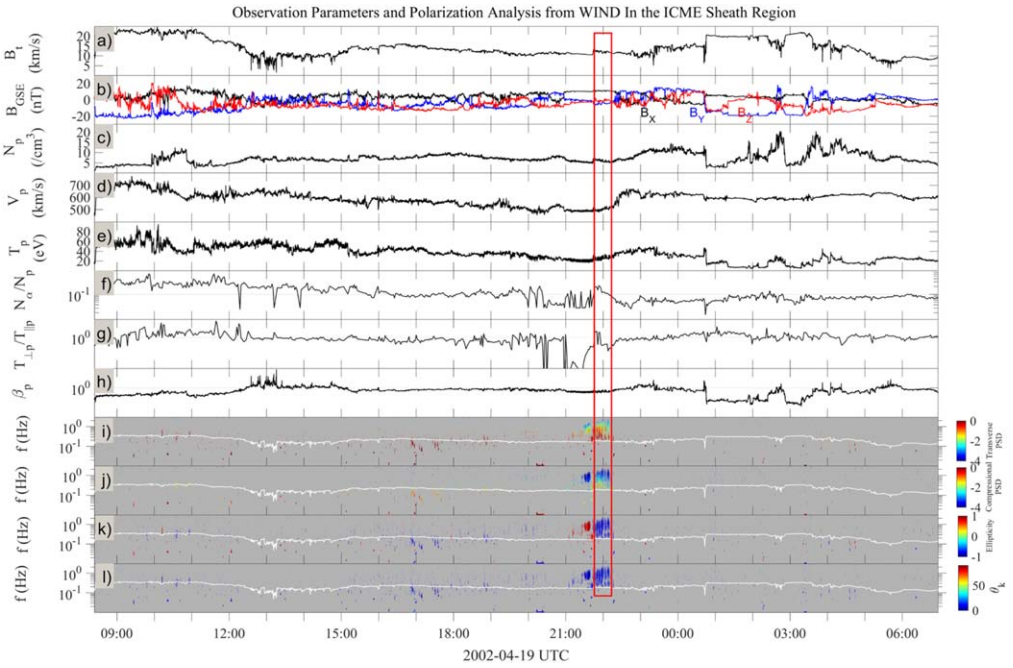

Figure 3. Observations of the sheath region of an ICME on 2002 April 19–20. The format is the same as that of Figure 1.

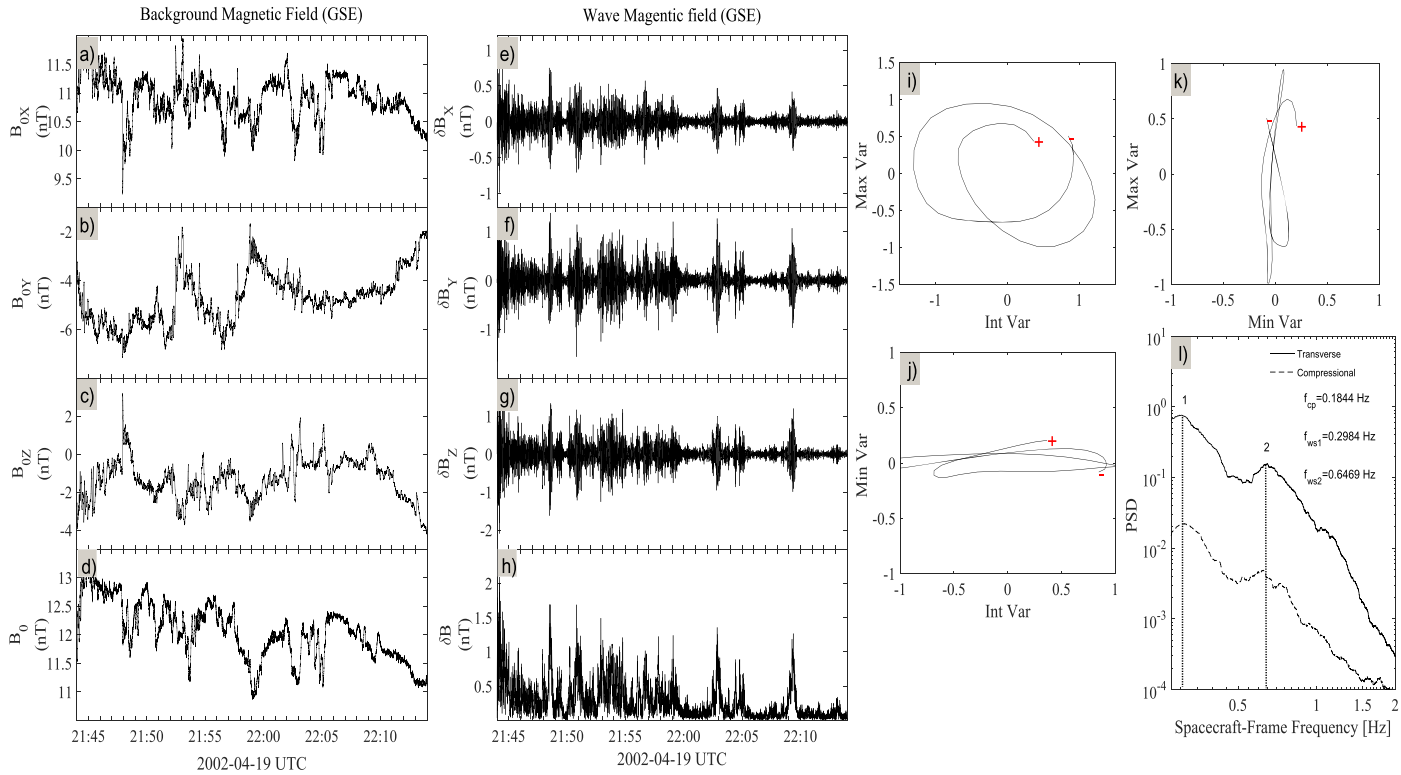

Figure 4. Characteristics of outward-propagating LH EMWs within a middle sheath region (i.e., the region marked by the red box in Figure 3). The format is the same as that of Figure 2. In Figure 4(i), $\boldsymbol{B}_0$ points into the paper.

Figure 3(f)) is larger than that in the solar wind, and the proton temperature anisotropy $T_{p\perp}/T_{p\parallel}$ (its mean value is 1.3346; see Figure 3(g)) is also higher than that in the solar wind.

Figure 4 shows an event of LH EMWs propagating outward within a middle sheath region, corresponding to the region marked by the red box in Figure 3. The time duration for this wave event is 30 minutes (21:44–22:14 on 2002 April 19). As can be seen from Figure 3(k), these EMWs are LH polarized in the spacecraft frame. Using repeated filtering analysis, we obtain the frequency range of the wave trains from $f_{\min} = 0.277$ Hz to $f_{\max} = 2$ Hz. Therefore, the frequency bandwidth Δf_{sc} for these EMWs is 1.723 Hz in the spacecraft frame. Figures 4(a)–(d) show the background magnetic field in the GSE coordinate system. The related wave field between $f_{\min}$ and $f_{\max}$ in the same coordinates is shown in Figures 4(e)–(h). The MVA for the wave field shows that the propagation angle $\theta_{\boldsymbol{kB}_0}$ is 1°.11. The

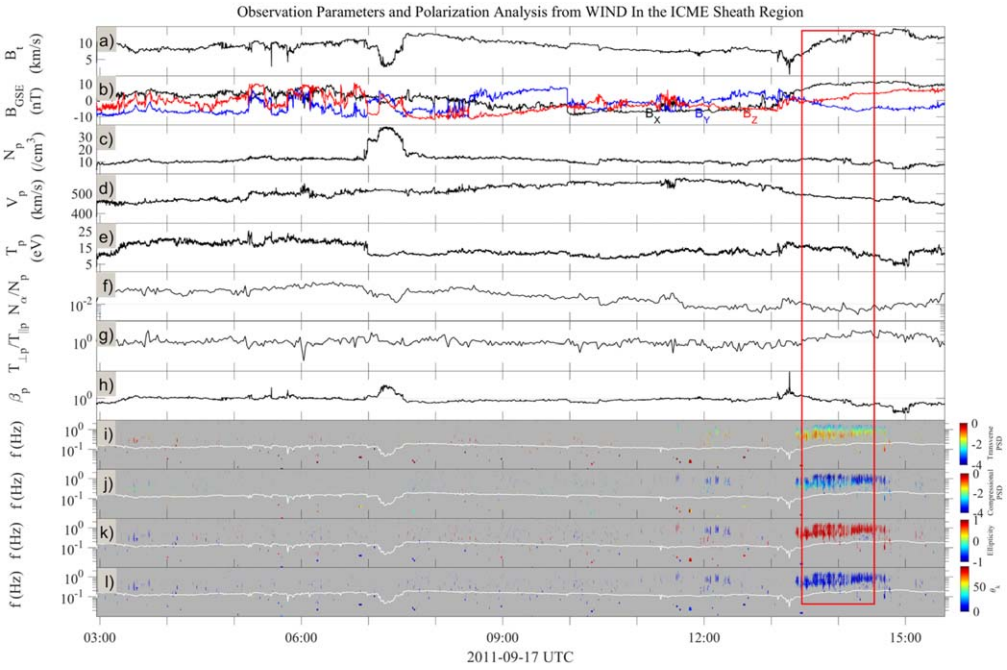

Figure 5. Observations of the sheath region of an ICME on 2011 September 17. The format is the same as that of Figure 1.

hodogram of the wave field $\delta \boldsymbol{B}$ in MVA coordinates is shown in Figures 4(i)–(k). Figure 4(i) indicates that these waves are LH polarized in the spacecraft frame, with the direction of $\boldsymbol{B}_0$ pointing into the paper. The ratio of the intermediate $\lambda_{\rm int}$ to the minimum $\lambda_{\rm min}$ eigenvalues is 11.4, indicating that these EMWs are plane waves.

The angle θ_{Ai} between $\boldsymbol{A}$ and $\boldsymbol{i}$ is 19°.7 in the SAK coordinate system, which means that the maximum variance direction of the wave field is nearly perpendicular to the $\boldsymbol{B}_0$–$\boldsymbol{k}$ plane. The characteristics of these waves are consistent with those of LH-polarized EMWs in the plasma frame. Comparing the wave polarization handedness in both spacecraft and plasma frames, we concluded that these waves are outward-propagating LH EMWs. The power spectral densities of the wave magnetic fields have two peak frequencies in the spacecraft frame, i.e., $f_{\rm ws1} = 0.2984$ Hz and $f_{\rm ws2} = 0.6469$ Hz (indicated by two vertical dotted lines in Figure 4(l)). After the Doppler effect is removed, the wave peak frequencies in the plasma frame are $f_{\rm wp1} \approx 0.048$ Hz and $f_{\rm wp2} \approx 0.104$ Hz, below the local proton cyclotron frequency $f_{\rm cp} = 0.1844$ Hz.

On the other hand, the mean value of $T_{\rm p\perp}/T_{\rm p\parallel}$ ($T_{\alpha\perp}/T_{\alpha\parallel}$) is 0.8371 (0.133). This implies that these outward-propagating LH EMWs may not be excited via the local proton (alpha) temperature anisotropy instability. But the excitation process of these EMWs through the local ion temperature anisotropy instability may be nearly finished when the local plasma develops into a relaxed state. Furthermore, the relative differential alpha-proton speed $V_{\rm d}/V_{\rm A}$ is 0.26. The average α abundance $N_\alpha/N_{\rm p}$ in this event is 25.33%, extremely higher than that in a typical solar wind.

2.3. EMWs near the ICME Leading Edge

Figure 5 shows an example of an ICME sheath region observed by the Wind spacecraft on 2011 September 17. The leading shock is at 02:57 UT, and the leading edge of the ICME is at 15:35 UT. For this ICME event, the leading shock angle θ_{Bn} is 73°.6, the Alfvén Mach number is 7.586, the fast magnetosonic Mach number is 1.4, and the upstream plasma beta β_1 is 0.236. It can be seen that the ICME leading shock is a fast and quasi-perpendicular shock. In the sheath region, we found a total of 16 EMW events, the total duration of which is 88.08 minutes, accounting for 11.62% of the duration of the whole sheath region (lasting 758 minutes). The dynamic spectral analysis of disturbed magnetic fields (see panels (i)–(l) in Figure 5) shows that most EMWs with frequencies higher than the local proton cyclotron frequency appear near the leading edge of the ICME or the trailing sheath region. In the whole sheath region, the mean value of the proton beta is 5.55 (Figure 5(h)), the mean relative α abundance $N_\alpha/N_{\rm p}$ is nearly 1.5% (Figure 5(f)) lower than that in the solar wind, and the proton temperature anisotropy $T_{\rm p\perp}/T_{\rm p\parallel}$ for most regions is isotropic (the mean value of $T_{\rm p\perp}/T_{\rm p\parallel}$ is 1.3346 in Figure 5(g)), except the region near the leading boundary of the ICME.

Figure 6 shows an example of inward-propagating LH EMWs within the trailing sheath region marked by the red box in Figure 5. The time duration of this wave event is 65 minutes (13:26–14:31 on 2011 September 17). These EMWs are RH polarized in the spacecraft frame (Figure 5(k)). After repeated filtering, we obtain the frequency range of the waves from $f_{\rm min} = 0.27$ Hz to $f_{\rm max} = 2$ Hz, and the related frequency bandwidth $\Delta f_{\rm sc}$ for this EMW event is 1.8 Hz in the spacecraft frame. Figures 6(a)–(d) show the background magnetic field in the GSE coordinate system. The wave field between $f_{\rm min}$ and $f_{\rm max}$ in the same coordinate system is displayed in Figures 6(e)–(h). The MVA of the wave magnetic field gives the wave propagation angle $\theta_{\boldsymbol{kB}_0} = 5°.898$ and a hodogram of the wave field $\delta \boldsymbol{B}$ in the MVA coordinate system (Figures 6(i)–(k)). These waves are RH polarized in the spacecraft frame with the direction of$\boldsymbol{B}_0$ pointing out of the paper (see Figure 6(i)). The ratio $\lambda_{\rm int}/\lambda_{\rm min}$ of intermediate to minimum eigenvalues is 4.286.

Accordingly, the angle θ_{Ai} is 8°.63, indicating that the characteristics of these waves are consistent with those of LH-polarized waves in the plasma frame. The opposite polarizations

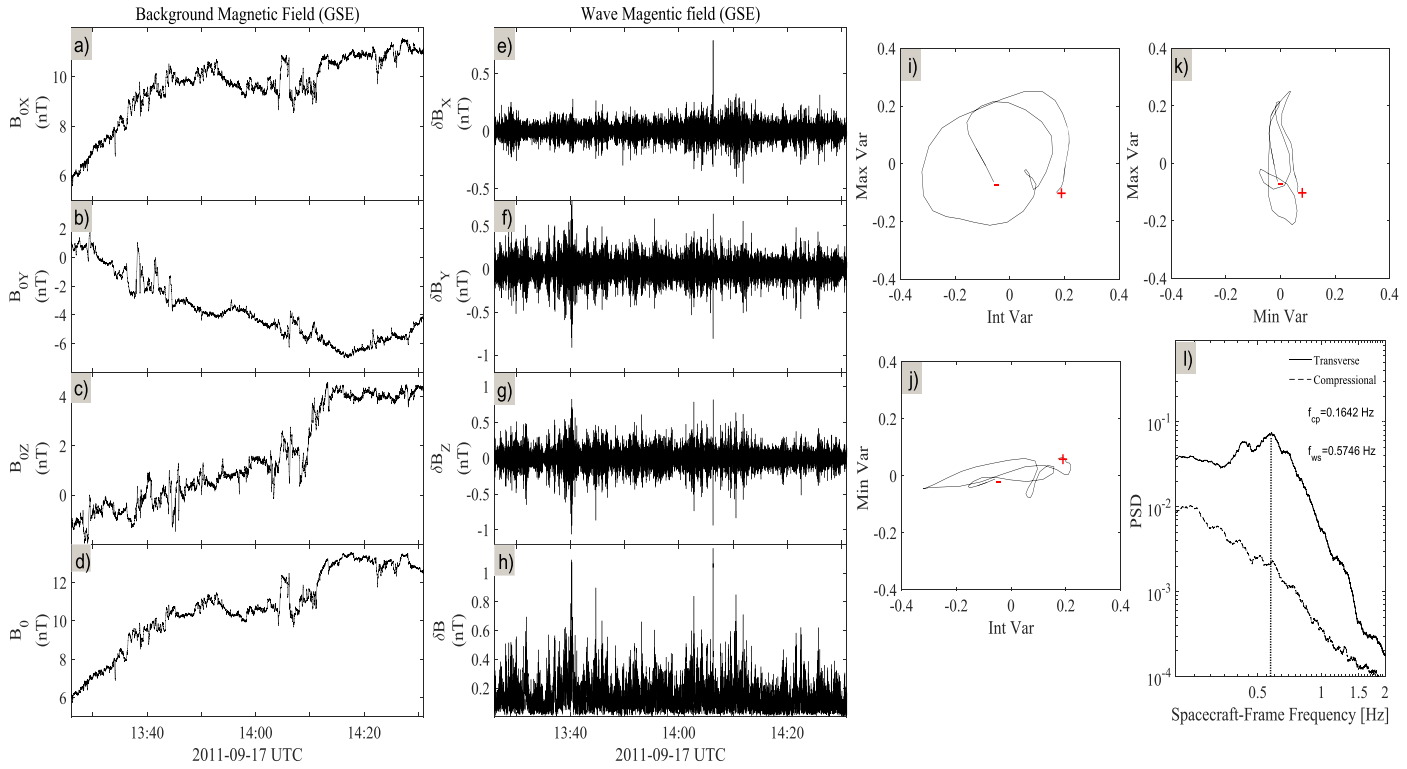

Figure 6. Characteristics of inward-propagating LH EMWs near the leading edge of an ICME (i.e., the region marked by the red box in Figure 5). The format is the same as that of Figure 2. In Figure 6(i), $\boldsymbol{B}_0$ points out of the paper.

of these EMWs in the spacecraft and plasma frames suggest the possibility that these waves are intrinsically inward-propagating LH EMWs. That is to say, the LH EMWs travel toward the leading edge of the ICME. The spectral analysis in Figure 6(l) shows that there is one peak frequency for this wave event in the spacecraft frame, i.e., $f_{\rm ws} = 0.5746$ Hz (indicated by the vertical dotted line in Figure 6(l)). After removing the Doppler effect of the solar wind flow, the wave peak frequency $f_{\rm wp} = 0.1049$ Hz in the plasma frame, below the local proton cyclotron frequency $f_{\rm cp} = 0.1642$ Hz.

On the other hand, the mean value of $T_{\rm p\perp}/T_{\rm p\parallel}$ ($T_{\alpha\perp}/T_{\alpha\parallel}$) is 1.8154 (1.6254), implying that these waves may be excited by the local proton (alpha) temperature anisotropy instability. By the time the measurements are made, the excitation process for these waves may not be over. Furthermore, the relative differential alpha-proton speed $V_{\rm d}/V_{\rm A}$ is 0.3377. The average α abundance $N_\alpha/N_{\rm p}$ in this event is 0.6%, much lower than that in the typical solar wind.

3. Statistical Analysis

According to the above case analyses, different locations in the ICME sheath region with different plasma environments could result in different mechanisms for wave excitation and dissipation. To understand the spatial distribution of these EMWs within the sheath regions, we normalize the wave event position to vary from 0 to 1, where the leading shock position is defined to be 0 and the leading edge position of the ICME to be 1. For a convenient description, the sheath regions are further divided into five parts: the front sheath region near the leading shock (0–0.2), the front of the middle sheath region (0.2–0.4), the center of the middle sheath region (0.4–0.6), the back of the middle sheath region (0.6–0.8), and the trailing sheath region near the leading edge of ICME (0.8–1).

Based on the lists of ICMEs and shocks observed by the Wind spacecraft (https://wind.nasa.gov/), a total of 62 ICME sheath regions with a leading quasi-perpendicular shock were selected for wave analysis in our statistical study. Among them, 31 ICMEs (50%) are magnetic clouds (MCs). The average and median velocities of these ICME sheath regions are 518.12 km s^{-1} and 493.19 km s^{-1}, respectively. Only 15 ICME sheath regions in our sample had velocities above 600 km s^{-1}. The plasma β of the ICME sheath regions ranges from 0.2 to 7.4, and its average and median values are 1.78 and 1.37, respectively. The proton temperature anisotropy $T_{\rm p\perp}/T_{\rm p\parallel}$ is greater than 1 for half the ICME sheath regions, and its average and median values are 1.37 and 1.05, respectively. Accordingly, the average and median values of $T_{\alpha\perp}/T_{\alpha\parallel}$ ($V_{\rm d}/V_{\rm A}$) are 4.85 (0.8) and 1.48 (0.63), respectively.

In these 62 sheath regions, we identified 700 EMW events, the total duration of which is 3001.1 minutes, accounting for 7.1% of the total analysis time. Each ICME sheath region contains at least one EMW event, and the greatest number of EMW events identified within a sheath region is 63, and the time duration of each wave event lasts at least 1 minute and can last up to 152.5 minutes. The total duration of EMWs ranges from 1.6 minutes to 601.533 minutes in a sheath region. Accordingly, the duration ratio between EMWs and the whole sheath region can vary from 0.35% to 67.12%. In the spacecraft frame, 397 EMW events with a total duration of 1713.1 minutes (56.7% of all identified EMW events) are LH-polarized EMWs, larger than that of RH-polarized EMWs. The corresponding number of RH EMW events are 303 with a total duration of 1288 minutes. However, in the plasma frame, the number (355 events) and duration (1545 minutes) of RH EMWs are slightly larger than the number (345 events) and duration (1456.1 minutes) of LH EMWs, respectively.

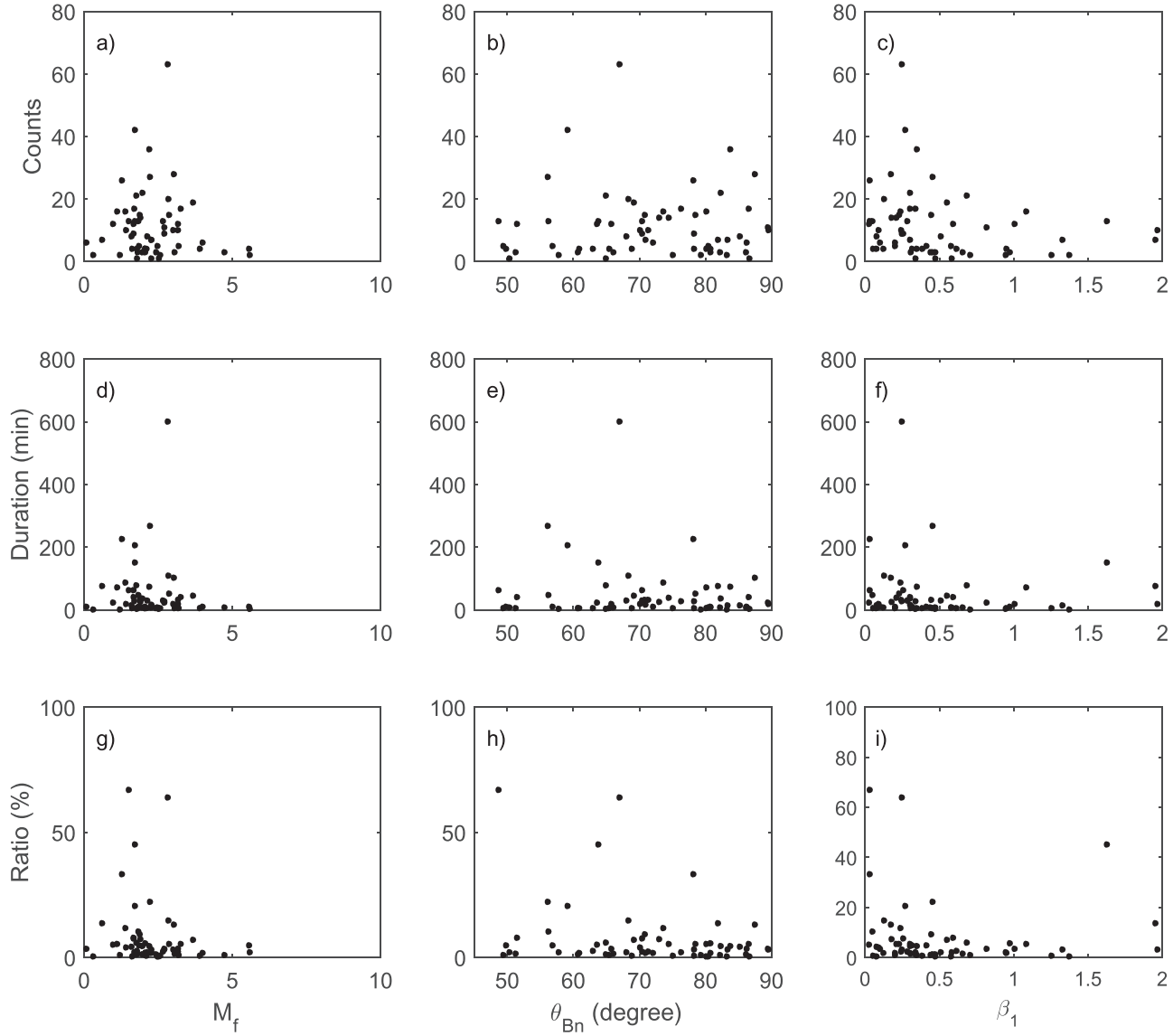

Figure 7. Scatter plots of the counts of EMW events ((a)–(c)), the duration of EMWs ((d)–(f)), and the duration ratio of EMW events to the associated sheath region ((g)–(i)) in the ICME sheath region vs. the leading quasi-perpendicular shock parameters (i.e., the fast Mach number M_f, the shock angle θ_{Bn}, and the upstream β_1).

3.1. Dependence of EMWs in ICME Sheath Regions on Shock Parameters

Figure 7 shows the scatter plots of the counts of EMW events, the duration of EMWs and the duration ratio of EMW events to the associated sheath region with the main parameters of quasi-perpendicular leading shocks (i.e., the fast Mach number M_f, the shock angle θ_{Bn}, and the upstream β_1) in ICME sheath regions. The shock parameters used here are from the shock list (https://www.cfa.harvard.edu/shocks/wi_data/). The average and the median fast Mach numbers M_f in our sample are 2.58 and 2.09, respectively. Figures 7(a), (d), and (g) show that the ICME sheath region associated with a low M_f leading shock is more favorable for EMWs. In the cases of our ICME sheath regions, the average and the median shock angles θ_{Bn} in our sample are 71°.35 and 71°.1, respectively. As can be seen from Figures 7(b), (e), and (h), the dependance of the occurrence rate of EMWs on the shock angle in the sheath region is not obvious. We also examined the relation between the upstream β1 and the occurrence rate of EMWs in the sheath region. The average and the median upstream β_1 in our sample are 0.4982 and 0.34, respectively. The values of upstream β_1 for about 87.1% of the ICME sheath regions are smaller than 1, which indicates that the sheath region with a low upstream β_1 is very conducive to the occurrence of EMWs.

3.2. Spatial Distributions of EMW Parameters in Spacecraft and Plasma Frames

To study the EMWs occurring at different locations of the ICME sheath regions, we divide an ICME sheath region into 10 subregions and then calculate the normalized position of EMW events, i.e., the center of the location where wave events occur. Figure 8 shows the spatial distributions of LH- (blue lines) and RH-EMW (red lines) parameters in both the spacecraft and plasma frames. Columns 1 and 2 in Figure 8 represent the spatial distributions in the spacecraft frame, while columns 3 and 4 represent those in the plasma frame. In each subregion, the median values of the corresponding parameters of EMWs are calculated for statistical analysis.

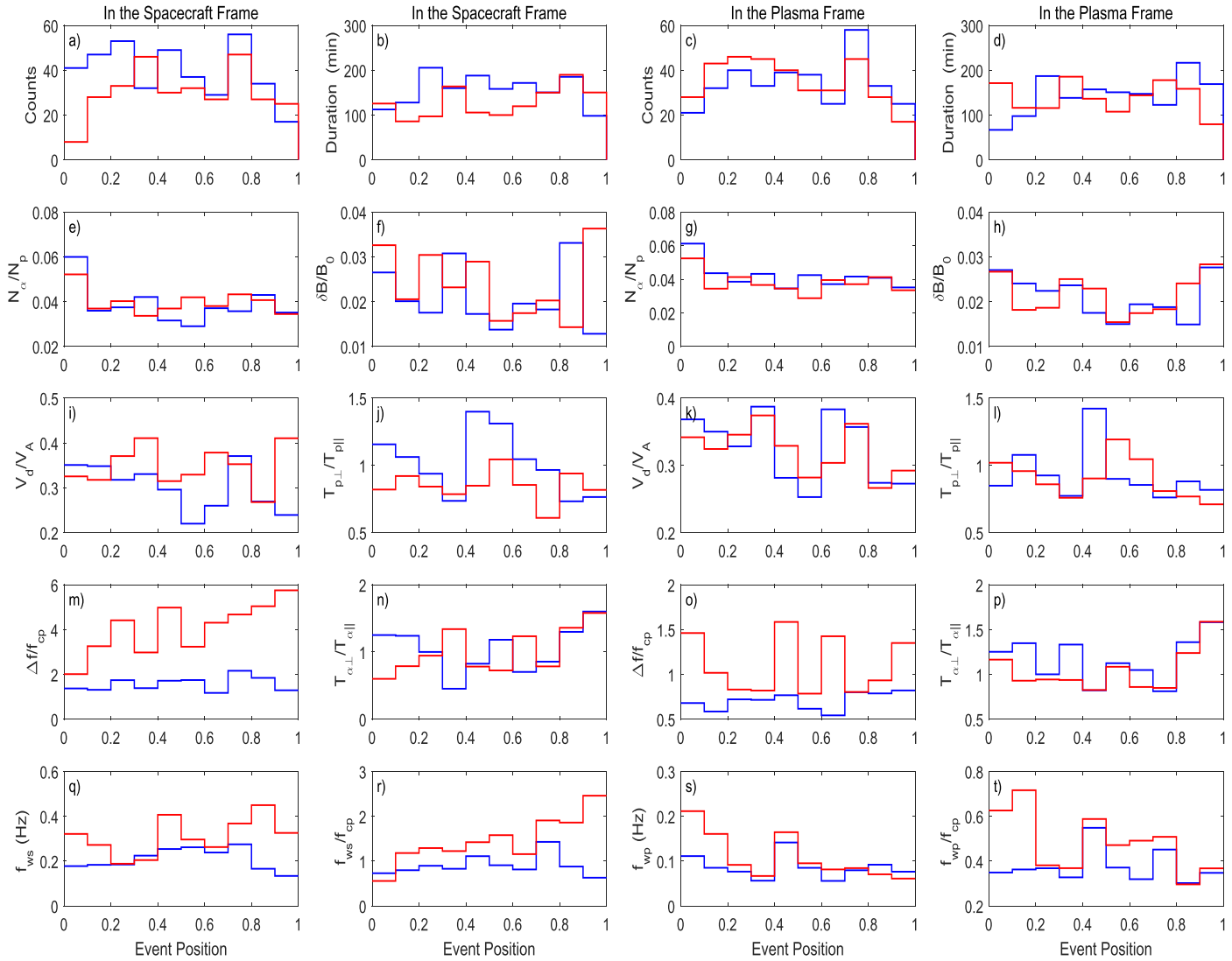

Figure 8. The spatial distributions of EMW-related parameters in both spacecraft (columns 1 and 2) and plasma (columns 3 and 4) frames, where the blue and red lines represent LH and RH EMWs, respectively. The parameters are the EMW counts ((a) and (c)), the duration of EMWs ((b) and (d)), the α abundance N_α/N_p ((e) and (g)), the relative wave amplitude $\delta B/B_0$ of EMWs ((f) and (h)), the normalized differential alpha-proton speed $V_\mathrm{d}/V_\mathrm{A}$ ((i) and (k)), the proton temperature anisotropy $T_{\mathrm{p}\perp}/T_{\mathrm{p}\parallel}$ ((j) and (l)), the normalized wave bandwidth $\Delta f/f_\mathrm{cp}$ of EMWs ((m) and (o)), the alpha temperature anisotropy $T_{\alpha\perp}/T_{\alpha\parallel}$ ((n) and (p)), the wave frequency $f_{\mathrm{ws(p)}}$ ((q) and (s)), and the normalized wave frequency $f_{\mathrm{ws(p)}}/f_\mathrm{cp}$ ((r) and (t)). The subscripts s and p in panels (q)–(t) represent the spacecraft and plasma frames, respectively.

Throughout most of the ICME sheath region (except the subregions (i.e., 0–0.1) near the leading shock, the front (i.e., 0.3–0.4) of the middle sheath region, and the back sheath region (i.e., 0.8–1) near the leading edge of the ICME), the LH EMWs have higher counts and longer durations than the RH EMWs in the spacecraft frame (Figures 8(a) and (b)). Although the counts of the RH EMWs in the spacecraft frame are much smaller than those of the LH EMWs in the sheath region near the leading shock (i.e., 0–0.1), the corresponding duration of the RH EMWs is longer than that of the LH EMWs. In the ICME sheath region near the leading edge of the ICME (i.e., 0.9–1), both counts and duration of the RH EMWs are higher than those of the LH EMWs in the spacecraft frame. Figures 8(c) and (d) show the spatial distributions of the counts and duration of the EMWs in the plasma frame. Compared with the counts of the LH EMWs in the plasma frame, the counts of the RH EMWs are higher in the first half of the sheath region and lower in most of the back half of the sheath region (Figure 8(c)). For the sheath region near the leading shock (i.e., 0–0.2), both counts and duration of the RH EMWs are larger than those of the LH EMWs in the plasma frame. In the back sheath region (0.8–1) near the leading edge of the ICME, however, the counts and duration of the LH EMWs are higher than those of the RH EMWs in the plasma frame (Figure 8(d)).

The spatial distributions of the magnetic field, plasma, and frequency parameters of EMWs are also presented in both spacecraft and plasma frames in ICME sheath regions (Figure 8). The relative wave amplitude $\delta B/B_0$ of the RH EMWs in the spacecraft (plasma) frame is larger (smaller) than that of the LH EMWs in the front sheath region (i.e., 0–0.3) near the leading shock shown by Figure 8(f) (Figure 8(h)), and the wave amplitude of the RH EMWs in the plasma frame is higher than that of the LH EMWs in both the middle sheath region (0.3–0.6) and the trailing sheath region (0.8–1) near the leading edge of ICME. It can be seen from Figures 8(e) and (g)

that the α abundance N_α/N_p of LH EMWs and RH EMWs in the sheath region (i.e., 0–0.1) near the leading shock in both spacecraft and plasma frames is higher than that in the other subregions of the ICME sheath.

Figures 8(m), (q), and (r) show the normalized wave bandwidth $\Delta f/f_{cp}$ of EMWs, the wave frequency f_{ws}, and the normalized wave frequency f_{ws}/f_{cp} in the spacecraft frame, respectively. After removing the Doppler effect of the solar wind flow, the normalized bandwidth $\Delta f/f_{cp}$ of EMWs, wave frequency f_{wp}, and the normalized wave frequency f_{wp}/f_{cp} in the plasma frame are also shown in Figures 8(o), (s), and (t), respectively. As can be seen from these six panels, the $\Delta f/f_{cp}$, f_{ws}, and f_{ws}/f_{cp} of RH EMWs are higher than those of the LH EMWs in most of the sheath region in both spacecraft and plasma frames. For LH EMWs in the plasma frame, the bandwidths are lower than the local proton cyclotron frequency f_{cp} throughout the sheath region (Figure 8(o)), and the wave frequency f_{wp} in most of the sheath regions is below $0.5f_{cp}$ (Figure 8(t)). On the contrary, RH EMWs in the plasma frame have larger bandwidths than LH EMWs almost throughout the whole sheath region (Figure 8(o)). Compared with the LH EMWs in the plasma frame, the RH EMWs have larger f_{wp} and f_{wp}/f_{cp} values in the front and middle sheath regions (i.e., 0–0.8).

In addition, we also performed a statistical analysis of the spatial distributions of the parameters associated with plasma instabilities in the ICME sheath regions, such as the normalized differential alpha-proton speed V_d/V_A (Figures 8(i) and (k)), the proton temperature anisotropy $T_{p\perp}/T_{p\parallel}$ (Figures 8(j) and (l)), and the alpha temperature anisotropy $T_{\alpha\perp}/T_{\alpha\parallel}$ (Figures 8(n) and (p)) in both spacecraft and plasma frames. In the front sheath regions (i.e., 0–0.2), the V_d/V_A, $T_{p\perp}/T_{p\parallel}$, and $T_{\alpha\perp}/T_{\alpha\parallel}$ for LH EMWs are all higher than those of RH EMWs in the spacecraft frame, and the last two parameters are all higher than 1 (Figures 8(i), (j), and (n)). Except $T_{p\perp}/T_{p\parallel}$, both the V_d/V_A and $T_{\alpha\perp}/T_{\alpha\parallel}$ of LH EMWs in the plasma frame are higher than those of RH EMWs in the front sheath regions (i.e., 0–0.2; see Figures 8(k), (l), and (p)). The $T_{p\perp}/T_{p\parallel}$ of the LH EMWs is greater than 1 in both spacecraft and plasma frames in the center (i.e., 0.4–0.5) of the middle sheath regions (Figures 8(j) and (l)). In both the front sheath region (i.e., 0–0.2) and the sheath region (i.e., 0.8–1) near the leading edge of the ICME, the $T_{\alpha\perp}/T_{\alpha\parallel}$ of LH EMWs in the plasma frame is also greater than 1 (Figure 8(p)). Besides, the $T_{\alpha\perp}/T_{\alpha\parallel}$ of LH EMWs in the plasma frame is larger than that of RH EMWs in most of the sheath subregions. On the other hand, both the $T_{p\perp}/T_{p\parallel}$ and $T_{\alpha\perp}/T_{\alpha\parallel}$ of RH EMWs in the plasma frame are less than 1 in most of the sheath subregions (Figures 8(l) and (p)).

3.3. Spatial Distributions of Inward- and Outward-propagating EMWs in the Sheath Regions

From the spacecraft to plasma frames, the polarization handedness of 330 EMW events in our study suffers a reversal in the sheath regions. Among these EMWs with polarization reversals, 19.86% (139 events with a total of 523.68 minutes) are LH EMWs and 27.3% (191 events with a total of 780.6 minutes) are RH EMWs in the plasma frame. The reason why the wave polarization is reversed is that the EMW propagation speed (~the Alfvén speed) is Doppler-shifted greatly by the solar wind speed with a typical Alfvén Mach number 5–8. These polarization-reversed EMWs could be interpreted to propagate toward the Sun in the solar wind and the remaining EMWs to propagate outward away from the Sun.

For outward-propagating LH EMWs, their counts and duration are 206 (accounting for 29.4% of all EMW events) and 932.45 minutes, respectively. For outward-propagating RH EMWs, the counts and duration are 164 (accounting for 23.43% of all EMW events) and 764.37 minutes, respectively. The outward-propagating LH EMWs and inward-propagating RH EMWs have relatively higher counts and duration than inward-propagating LH EMWs and outward-propagating RH EMWs in the plasma frame, respectively. These results are consistent with our previous statistical results using STEREO spacecraft data (Li et al. 2019).

Figure 9 shows the spatial distributions of inward- and outward-propagating EMWs with the normalized event position in the sheath region. Columns 1 and 2 represent the distributions of the outward-propagating EMWs, and columns 3 and 4 the distributions of the inward-propagating EMWs. For each panel in Figure 9, the blue line represents the LH EMWs, and the red line the RH EMWs. Throughout most of the ICME sheath region (except the sheath subregion (i.e., 0–0.1) near the leading shock, the front (i.e., 0.3–0.4) of the middle sheath region, and the back (i.e., 0.7–0.8) of the middle sheath region), the outward-propagating LH EMWs have higher counts and longer duration than outward-propagating RH EMWs in Figures 9(a) and (b). Although the counts of outward-propagating RH EMWs are much smaller than that of outward-propagating LH EMWs in the sheath subregion (i.e., 0–0.1) near the leading shock, the duration of outward-propagating RH EMWs is longer than that of outward-propagating LH EMWs. In the front (i.e., 0.3–0.4) of the middle sheath region, both counts and duration of the outward-propagating RH EMWs are higher than those of the outward-propagating LH EMWs.

Figures 9(c) and (d) show the spatial distributions of the counts and durations of inward-propagating EMWs. Both the counts and duration of the inward-propagating RH EMWs are higher than those of the LH EMWs in most ICME sheath regions, shown by Figures 9(c) and (d), especially in the sheath subregion (i.e., 0–0.3) near the leading shock. However, in the sheath subregion (i.e., 0.9–1) near the leading edge of the ICME, the counts and duration of inward-propagating LH EMWs are higher than those of inward-propagating RH EMWs.

In the sheath subregion (i.e., 0–0.1) near the leading shock, it can be seen from Figures 9(e) and (g) that the α abundance N_α/N_p of both outward- and inward- propagating EMWs are higher than the other sheath regions. Figures 9(m), (q), and (r) show the $\Delta f/f_{cp}$, f_{wp}, and f_{wp}/f_{cp} of the outward-propagating EMWs, respectively. The frequency bandwidth $\Delta f/f_{cp}$ of the outward-propagating RH EMWs is wider than that of the outward-propagating LH EMWs in nearly the whole sheath region (Figure 9(m)). For outward-propagating LH EMWs, the bandwidths $\Delta f/f_{cp}$ and the related wave frequency f_{wp}/f_{cp} in the plasma frame are smaller than the local proton cyclotron frequency f_{cp} and $0.5f_{cp}$ throughout the sheath region, shown in Figures 9(m) and (r), respectively. The parameters $\Delta f/f_{cp}$, f_{wp}, and f_{wp}/f_{cp} of the inward-propagating EMWs are shown in Figures 9(o), (s) and (t), respectively. Both the $\Delta f/f_{cp}$ and f_{wp}/f_{cp} of inward-propagating LH EMWs are higher than those of outward-propagating LH EMWs in most of the sheath subregions (Figures 9(m), (o), (r), and (t)).

Figures 9(i) and (k) show the spatial distributions of the relative differential alpha-proton speed V_d/V_A, Figures 9(j) and (l) the

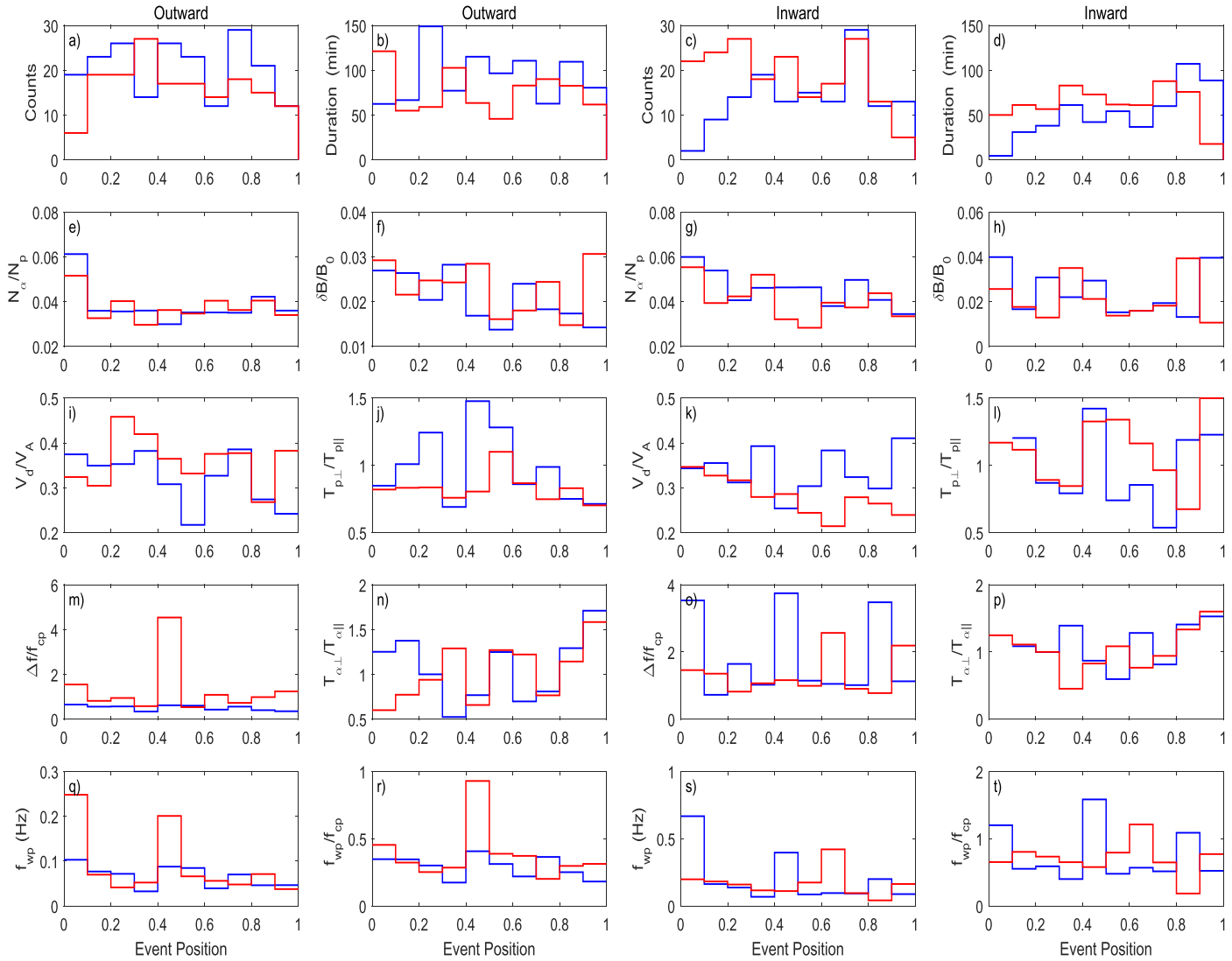

Figure 9. The spatial distributions of inward-propagating and outward-propagating EMWs in the plasma frame in ICME sheath regions. The format is the same as in Figure 8.

spatial distributions of the proton temperature ratio $T_{p\perp}/T_{p\parallel}$, and Figures 9(n) and (p) the spatial distributions of the α temperature ratio $T_{\alpha\perp}/T_{\alpha\parallel}$. In the sheath region (i.e., 0–0.2) near the leading shock, the α abundance N_α/N_p, V_d/V_A, $T_{p\perp}/T_{p\parallel}$, and $T_{\alpha\perp}/T_{\alpha\parallel}$ of the outward-propagating LH EMWs are all larger than those of the outward-propagating RH EMWs (Figures 9(e), (i), (j), and (n)), and the $T_{\alpha\perp}/T_{\alpha\parallel}$ of the outward-propagating LH EMWs is higher than 1 in this region (Figure 9(n)). The proton temperature ratio $T_{p\perp}/T_{p\parallel}$ of both outward- and inward-propagating LH EMWs is greater than 1 in the center (i.e., 0.4–0.5) of the middle sheath region (Figures 9(j) and (l)).

4. Discussion

What are the excitation mechanisms of these EMWs in the ICME sheath regions? The question still remains unanswered. The magnetic field and plasma have different environments within the ICME sheath regions, where there are multiple possible sources of EMWs: the upstream solar wind fluctuations, the convected foreshock waves passing through the leading shock, waves generated by the leading shock or inside ICMEs, and waves excited locally in the sheath regions.

First, from the statistical results of the leading shock parameters, the occurrence of EMWs favors those sheath regions with relatively low M_f and low upstream β_1. Both observations and 2D hybrid simulations show that ion cyclotron waves are dominant in the downstream of the quasi-perpendicular shock with a low Mach number and low $\beta 1$ (Anderson et al. 1991; Anderson & Fuselier 1993; McKean et al. 1995, 1996; Russell & Farris 1995; Lu & Wang 2006). For a low M_f shock (McKean et al. 1996); the proton cyclotron waves are excited near the shock front and are then convected to the downstream, which may be a possible excitation mechanism of the inward-propagating LH EMWs near the leading shock in Figure 2. The proton cyclotron waves can be an energy source for the helium cyclotron waves through perpendicular helium temperature anisotropy (McKean et al. 1995, 1996). On the other hand, due to the different charge-to-mass ratios between proton and alpha particles, a ring-beam distribution of alpha particles can be formed downstream of a quasi-perpendicular shock (Fuselier & Schmidt 1997; Lu & Wang 2006). Both the

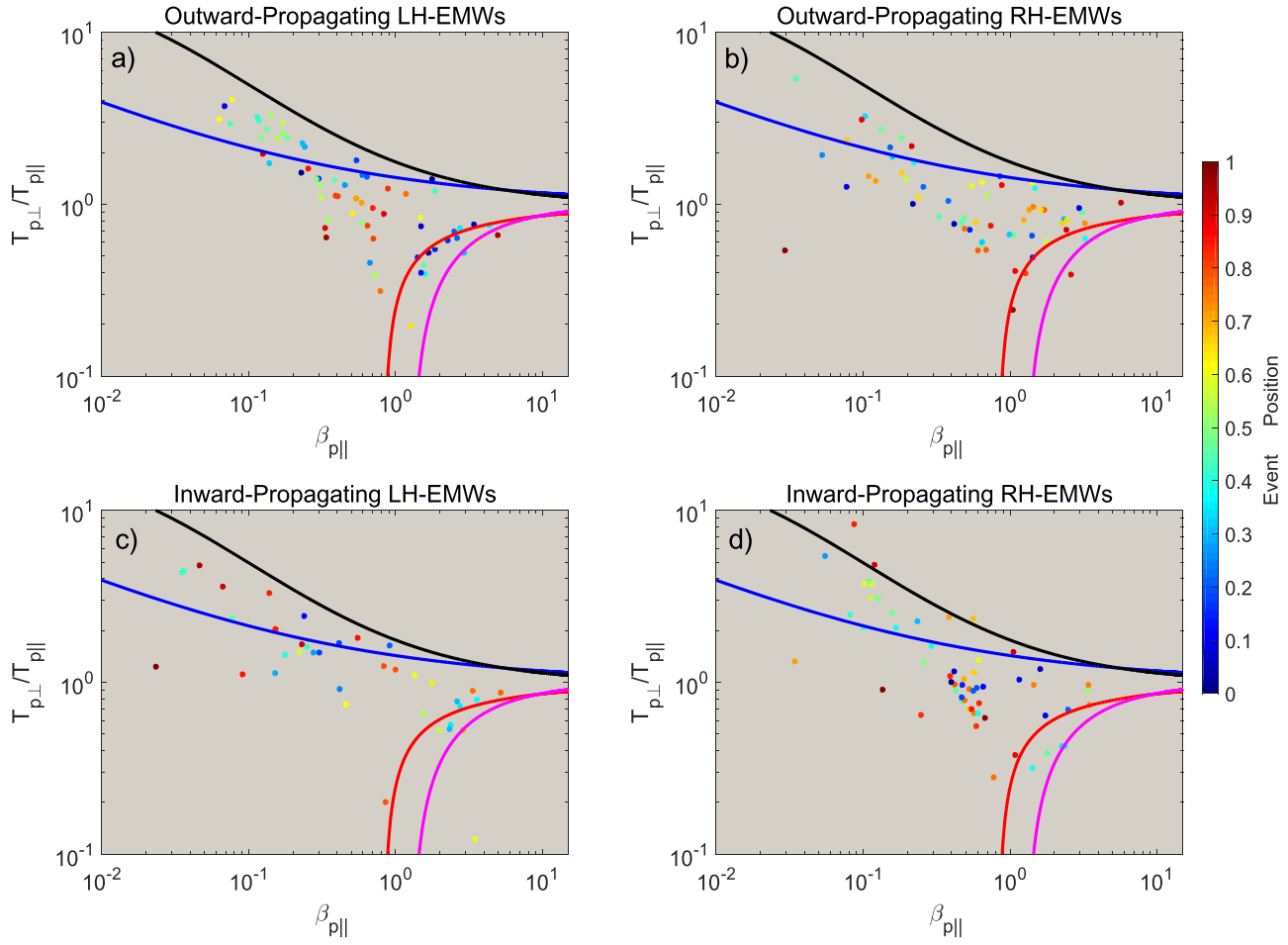

Figure 10. Scatter plots of proton temperature anisotropy $T_{p\perp}/T_{p||}$ against parallel proton beta $\beta_{p||}$ for inward- and outward-propagating EMWs with LH and RH polarizations in the ICME sheath regions. The color bar shows the position of the EMW event in the sheath region (0 = leading shock position, 1 = leading edge of ICME). Solid blue and red curves show the instability thresholds for the proton cyclotron anisotropy and parallel proton firehose instabilities, respectively. Solid black and magenta curves show the thresholds for the proton mirror and oblique proton firehose instabilities, respectively.

ring-beam and shell-like distributions of helium ions have been observed in the downstream of a quasi-perpendicular shock (Fuselier et al. 1988; Fuselier & Schmidt 1994, 1997; Lee & Wu 2000; Lee 2001), which makes it possible for the excitation of helium cyclotron waves (Gary et al. 1994; Lu & Wang 2006). Hao et al. (2014) demonstrated that α particles show a bunched ring-like distribution in the downstream of quasi-perpendicular shocks, which can excite helium cyclotron waves in the medium and low Mach number shocks, scattering helium ions into a shell-like distribution. Finally, a nearly bi-Maxwellian distribution is formed far downstream of the shocks.

Although the EMWs driven by proton temperature anisotropy have been extensively studied (Hellinger et al. 2006; Bale et al. 2009; Maruca et al. 2012; Yoon 2017), their excitation mechanisms may not necessarily be unique. Previous studies on ion temperature anisotropy have demonstrated that there is an inverse relationship between $T_{i\perp}/T_{i||}$ and $\beta_{i||}$, describing the variation of phase-space instability thresholds (Anderson & Fuselier 1993; Hellinger et al. 2006; Bale et al. 2009; Maruca et al. 2012; Bourouaine et al. 2013). Simulations have shown that for plasma conditions above the instability thresholds, the wave emission and the diffusion of perpendicular to parallel energy can reduce $T_{\perp i}/T_{||i}$ to below the threshold or at least to a value balanced by the physical processes driving increases in $T_{\perp i}/T_{||i}$ (Gary et al. 1997, 2006; Araneda et al. 2008).

In order to explore the excitation mechanisms of these EMWs in the ICME sheath regions, we will further examine the spatial distributions of local ion (i.e., protons and alphas) temperature anisotropy of the subregions containing EMWs. Figures 10 and 11 present the EMW event position in the ($\beta_{p||}$, $T_{p\perp}/T_{p||}$) and ($\beta_{\alpha||}$, $T_{\alpha\perp}/T_{\alpha||}$) planes, respectively. The color bars in Figures 10 and 11 show the positions of EMW events in the sheath region from the leading shock (i.e., position = 0) to the leading edge of ICME (i.e., position = 1). The solid blue lines show the threshold for the proton (alpha) temperature anisotropy instability, the solid black lines show the threshold for the proton (alpha) mirror instability, the solid magenta lines show the threshold for the oblique proton (alpha) firehose instability, and the solid red lines show the threshold for the parallel proton (alpha) firehose instability (Hellinger et al. 2006; Maruca et al. 2012). Due to the low-resolution alpha and proton anisotropy data, EMWs lasting more than three minutes in the sheath subregions are selected to make the results more reliable in our analysis.

As can be seen from Figures 10 and 11, most LH EMWs (RH EMWs) are below the thresholds of the ion temperature (parallel

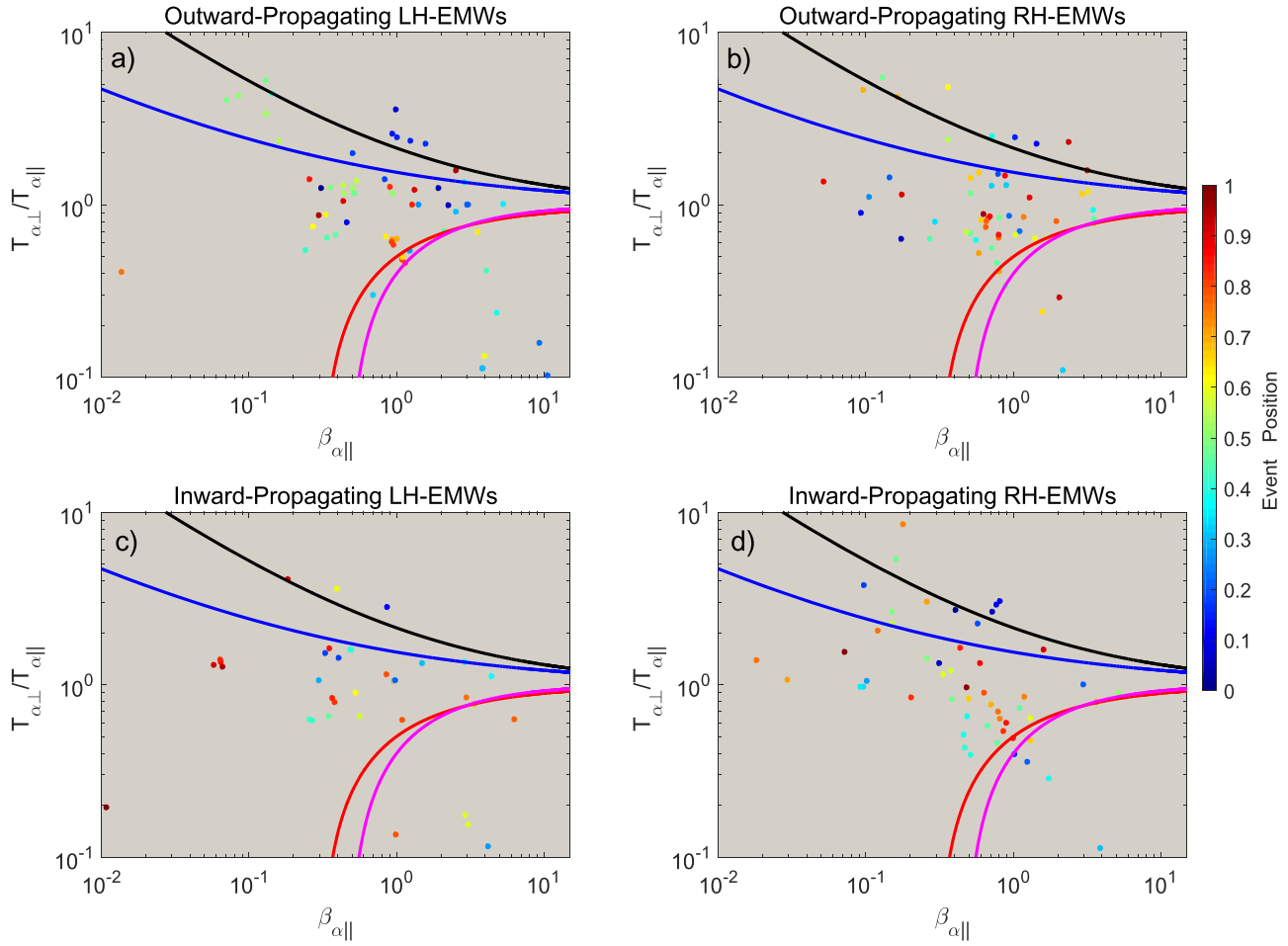

Figure 11. Scatter plots of alpha temperature anisotropy $T_{\alpha\perp}/T_{\alpha\parallel}$ against parallel α beta $\beta_{\alpha\parallel}$ for inward- and outward-propagating EMWs with LH and RH polarizations in the ICME sheath regions. The color bar shows the position of the EMW event in the sheath region (0 = leading shock position, 1 = leading edge of ICME). Solid blue and red curves show the instability thresholds for the alpha cyclotron anisotropy and parallel alpha firehose instabilities, respectively. Solid black and magenta curves show the thresholds for the alpha mirror and oblique alpha firehose instabilities, respectively.

ion firehose) instabilities in nearly the whole ICME sheath subregions, especially the RH EMWs. From Figure 10(a), we can see that $T_{p\perp}/T_{p\parallel}$ and $\beta_{p\parallel}$ for some outward-propagating LH EMWs in the middle sheath region are above (below) the threshold of the proton temperature (mirror) instability, which is consistent with the statistical results in Figure 9(j). Combining the results of Figures 10(a) and 9(j), the local proton temperature instability in the middle sheath regions could provide free energy to excite outward-propagating LH EMWs. For some outward-propagating LH EMWs near the leading shock, the related local alpha temperature anisotropy is above the thresholds of both the alpha temperature anisotropy and mirror instabilities (Figure 11(a)), which is consistent with the statistical results in Figure 9(n). From Figures 9(r) and (t), the normalized frequencies of the outward-propagating LH EMWs near the leading shock are below the local alpha cyclotron frequency, but the frequencies of the inward-propagating LH EMWs are around the local proton cyclotron frequency. Combining the results of Figures 9(r) and 11(a), it could be inferred that the outward-propagating LH EMWs near the leading shock are helium cyclotron waves and excited by the local alpha temperature anisotropy instability. The free energy source of the instability may be alpha particles that gain energy from the high-frequency inward-propagating LH EMWs.

For both inward- and outward-propagating RH EMWs, it seems that the local parallel ion firehose instabilities are in a stable state (Figures 10(b) and (d), 11(b) and (d)). It indicates that the excitation of RH EMWs in the ICME sheath regions may be not due to local ion parallel firehose instabilities, but possibly due to ion beams in the ICME sheath regions. In the present study, 47.3% of EMW events have an alpha abundance N_α/N_p larger than 0.04 (the typical value of the abundance in solar wind). Previous research show that the α abundance N_α/N_p may play an important role in the generation, propagation, and absorption of EMWs, and the resulting ion scattering and heating (Price et al. 1986; Liu et al. 2006; Zhao et al. 2019). Due to the existence of a differential alpha-proton speed V_d/V_A in the ICME sheath regions, the ion temperature anisotropy and parallel firehose instabilities may prefer outward-propagating LH EMWs and inward-propagating RH EMWs, respectively (Podesta & Gary 2011; Verscharen et al. 2013).

Although the interplanetary shocks ahead of the ICME sheath regions are all quasi-perpendicular shocks in our samples, the plasma in the ICME sheath regions is not always characterized by a larger perpendicular temperature anisotropy ($T_{p\perp}/T_{p\parallel} > 1$; see panel (g) in Figures 1, 3, 5). Unlike planetary magnetosheaths, ICME sheath regions are expanding in the solar wind, and one would expect that $T_{p\perp} < T_{p\parallel}$, due to the conservation of magnetic moment of the ions in a decreasing radial magnetic field. Such an instability can regulate the temperature anisotropy of solar wind protons by exciting RH EMWs.

5. Summary and Conclusions

The ICME sheath region is a natural laboratory to study EMWs and their properties. The motivation for this study mainly stems from the fact that the variations of the magnetic field and plasma in the ICME sheath regions are considerably larger than those in the ICMEs and solar wind, developing different plasma environments with different mechanisms for the excitation and dissipation of EMWs. Using the magnetic field and plasma data obtained from the Wind spacecraft, including 92 s solar wind alpha and proton temperature anisotropy data, we investigate the statistical properties of EMWs and their spatial distribution characteristics within 62 ICME sheath regions associated with quasi-perpendicular shocks. We also compare the spatial distribution characteristics of LH EMWs and RH EMWs in both spacecraft and plasma frames. As far as we know, it is the first attempt to systematically study the spatial distribution characteristics of EMWs in the sheath regions between quasi-perpendicular interplanetary shocks and ICMEs. Here we briefly summarize the main results of our work:

1. The ICME sheath region associated with a quasi-perpendicular leading shock which has a low M_f and a low upstream β_1 is very conducive to the occurrence of EMWs. The relation between the shock angle and the occurrence of EMWs in the ICME sheath region is not obvious.
2. In the spacecraft frame, the LH EMWs have higher counts and longer duration than RH EMWs in most ICME sheath subregions, except those near the ICME leading edge, but in the subregions near the leading shock, the RH EMWs have a longer duration than the LH EMWs. In the plasma frame, the RH EMWs have higher counts and longer duration than the LH EMWs in the subregions near the leading shock, but the counts and duration of LH EMWs are higher than those of the RH EMWs in the subregions near the leading edge of ICMEs.
3. In both spacecraft and plasma frames, the normalized wave bandwidth $\Delta f/f_{cp}$, the wave frequency $f_{ws(p)}$, and the normalized wave frequency $f_{ws(p)}/f_{cp}$ of RH EMWs are higher than those of LH EMWs in most of the sheath region, and the α abundance N_α/N_p of LH EMWs and RH EMWs in the subregion near the leading shock is higher than that in a typical solar wind. The $\Delta f/f_{cp}$ (f_{wp}) of LH EMWs in the plasma frame are lower than f_{cp} ($0.5f_{cp}$) in most of the sheath regions.
4. In sheath subregions near the leading shock and the ICME leading edge, the alpha temperature anisotropy $T_{\alpha\perp}/T_{\alpha\parallel}$ for LH EMWs in the plasma frame is greater than 1. The proton temperature anisotropy $T_{p\perp}/T_{p\parallel}$ of the LH EMWs is greater than 1 in both spacecraft and plasma frames in the center of the middle sheath regions. On the other hand, both $T_{p\perp}/T_{p\parallel}$ and $T_{\alpha\perp}/T_{\alpha\parallel}$ of RH EMWs in the plasma frame are less than 1 in most sheath regions.
5. In the sheath region near the leading shock, the α abundance N_α/N_p, the normalized differential alpha-proton speed V_d/V_A, the proton temperature anisotropy $T_{p\perp}/T_{p\parallel}$, and the alpha temperature anisotropy $T_{\alpha\perp}/T_{\alpha\parallel}$ of the outward-propagating LH EMWs are larger than those of the outward-propagating RH EMWs, and the $T_{\alpha\perp}/T_{\alpha\parallel}$ of the outward-propagating LH EMWs is higher than 1 in the sheath regions. The proton temperature ratio $T_{p\perp}/T_{p\parallel}$ of both outward- and inward-propagating LH EMWs is greater than 1 in the center of the middle sheath region.
6. Most EMWs have frequencies below the local proton cyclotron frequency. The wave frequency for most outward-propagating LH EMWs (81.1% of all outward-propagating LH EMWs) is smaller than $0.5f_{cp}$, and more than half of the inward-propagating LH EMWs have a frequency greater than $0.5f_{cp}$ (59% of all inward-propagating LH EMWs in the plasma frame). For outward (inward)-propagating RH EMWs, 68.3% (64%) RH EMWs have a frequency smaller (greater) than $0.5f_{cp}$.

In summary, based on the statistical analysis of EMWs within the ICME sheath regions and the related discussions about the excitation mechanism, our results show that the excitation mechanism of outward-propagating LH EMWs near the leading shock and the leading edge of ICMEs may be the local alpha temperature anisotropy instability. In the middle sheath region, the local proton temperature anisotropy instability may excite outward-propagating LH EMWs. The excitation source of inward-propagating LH EMWs may be from the leading shock or the earlier phases of the sheath regions. On the other hand, when the local plasma is near quasilinear saturation state during the measurements, it may not be appropriate to use the measured field and plasma data to deduce related plasma instabilities or the wave excitation mechanisms. Furthermore, the alpha-proton differential speed and the alpha abundance may have important effects on the excitation of EMWs in the ICME sheath regions (Podesta & Gary 2011; Verscharen et al. 2013).

This work was supported in part by the NSFC under grants 41531071, 41874201, 11873018, 11790302, and 11761131007. We thank the Wind team and NASA's CDAWeb for making these data available. The authors also would like to thank Drs. J.S. Zhao, Y.F. Hao, and H.Y. Sun for their useful suggestions and discussions.

ORCID iDs

D. J. Wu https://orcid.org/0000-0003-2418-5508

References

Ala-Lahti, M., Kilpua, E. K. J., Souček, J., et al. 2019, JGRA, 124, 3893
Allen, R. C., Zhang, J.-C., Kistler, L. M., et al. 2015, JGRA, 120, 5574
Anderson, B. J., & Fuselier, S. A. 1993, JGR, 98, 1461
Anderson, B. J., Fuselier, S. A., & Murr, D. 1991, GeoRL, 18, 1955
Araneda, J. A., Marsch, E., & F.-Viñas, A. 2008, PhRvL, 100, 125003
Bale, S. D., Balikhin, M. A., Horbury, T. S., et al. 2005, SSRv, 118, 161
Bale, S. D., Kasper, J. C., Howes, G. G., et al. 2009, PhRvL, 103, 211101
Blanco-Cano, X., & Schwartz, S. J. 1995, AdSpR, 15, 97
Boardsen, S. A., Jian, L. K., Raines, J. L., et al. 2015, JGRA, 120, 10207
Bourouaine, S., Marsch, E., & Neubauer, F. M. 2011, ApJL, 728, L3
Bourouaine, S., Verscharen, D., Chandran, B. D. G., et al. 2013, ApJL, 777, L3
Burgess, D., Lucek, E. A., Scholer, M., et al. 2005, SSRv, 118, 205
Burlaga, L. F. 1988, JGR, 93, 7217
Burlaga, L. F., Klein, L., Sheeley, N. R., et al. 1982, GeoRL, 9, 1317
Cane, H. V. 1988, JGR, 93, 1
Convery, P. D., & Gary, S. P. 1997, JGR, 102, 2351
Crooker, N., Joselyn, J. A., & Feynman, J. 1997, GMS, 99
Crooker, N. U., & Horbury, T. S. 2006, SSRv, 123, 93
Crooker, N. U., & Siscoe, G. L. 1977, JGR, 82, 185
Denskat, K. U., Beinroth, H. J., & Neubauer, F. M. 1983, JGZG, 54, 60
Forbes, T. G. 2000, JGR, 105, 23153
Fuselier, S. A., & Schmidt, W. K. H. 1994, JGR, 99, 11539
Fuselier, S. A., & Schmidt, W. K. H. 1997, JGR, 102, 11273
Fuselier, S. A., Shelley, E. G., & Klumpar, D. M. 1988, GeoRL, 15, 1333
Gary, S. P. 1993, Theory of Space Plasma Microinstabilities (Cambridge: Cambridge Univ. Press)

Gary, S. P., Goldstein, B. E., & Steinberg, J. T. 2001, JGR, 106, 24955
Gary, S. P., Jian, L. K., Broiles, T. W., et al. 2016, JGRA, 121, 30
Gary, S. P., McKean, M. E., Winske, D., et al. 1994, JGR, 99, 5903
Gary, S. P., Montgomery, M. D., Feldman, W. C., et al. 1976, JGR, 81, 1241
Gary, S. P., Wang, J., Winske, D., et al. 1997, JGR, 102, 27159
Gary, S. P., Yin, L., Winske, D., et al. 2003, JGRA, 108, 1068
Gary, S. P., Yin, L., & Winske, D. 2006, JGRA, 111, A06105
Good, S. W., Forsyth, R. J., Raines, J. M., et al. 2015, ApJ, 807, 177
Guo, J., Feng, X., Emery, B. A., et al. 2011, JGRA, 116, A05106
Hamilton, K., Smith, C. W., Vasquez, B. J., et al. 2008, JGRA, 113, A01106
Hao, Y., Lu, Q., Gao, X., et al. 2014, JGRA, 119, 3225
Hao, Y., Lu, Q., Gao, X., et al. 2016, ApJ, 823, 7
Hellinger, P., Trávníček, P., Kasper, J. C., et al. 2006, GeoRL, 33, L09101
Howard, R. A., Sheeley, N. R., Michels, D. J., et al. 1985, JGR, 90, 8173
Howard, T. A., & Tappin, S. J. 2009, SSRv, 147, 31
Huttunen, K., & Koskinen, H. 2004, AnGeo, 22, 1729
Huttunen, K. E. J., Koskinen, H. E. J., & Schwenn, R. 2002, JGRA, 107, 1121
Janvier, M., Démoulin, P., & Dasso, S. 2014, A&A, 565, A99
Jian, L. K., Russell, C. T., Luhmann, J. G., et al. 2009, ApJL, 701, L105
Jian, L. K., Russell, C. T., Luhmann, J. G., et al. 2010, JGRA, 115, A12115
Jones, G. H., Rees, A., Balogh, A., et al. 2002, GeoRL, 29, 1520
Kajdič, P., Blanco-Cano, X., Aguilar-Rodriguez, E., et al. 2012, JGRA, 117, A06103
Kasper, J. C. 2002, PhD thesis, Massachusetts Institute of Technology
Kasper, J. C., Lazarus, A. J., Steinberg, J. T., et al. 2006, JGRA, 111, A03105
Kasper, J. C., Maruca, B. A., Stevens, M. L., et al. 2013, PhRvL, 110, 091102
Kataoka, R., Watari, S., Shimada, N., et al. 2005, GeoRL, 32, L12103
Kaymaz, Z., & Siscoe, G. 2006, SoPh, 239, 437
Kilpua, E., Koskinen, H. E. J., & Pulkkinen, T. I. 2017, LRSP, 14, 5
Kilpua, E. K. J., Hietala, H., Koskinen, H. E. J., et al. 2013, AnGeo, 31, 1559
Klecker, B., Kunow, H., Cane, H. V., et al. 2006, SSRv, 123, 217
Klein, K. G., Alterman, B. L., Stevens, M. L., et al. 2018, PhRvL, 120, 205102
Krauss-Varban, D., & Omidi, N. 1991, JGR, 96, 17715
Kuramitsu, Y., & Krasnoselskikh, V. 2005, JGRA, 110, A10108
Leamon, R. J., Matthaeus, W. H., Smith, C. W., et al. 2000, ApJ, 537, 1054
Lee, L. C. 2001, SSRv, 95, 95
Lee, L. C., Price, C. P., Wu, C. S., et al. 1988, JGR, 93, 247
Lee, L. C., & Wu, B. H. 2000, ApJ, 535, 1014
Lembege, B., Giacalone, J., Scholer, M., et al. 2004, SSRv, 110, 161
Lepping, R. P., Acũna, M. H., Burlaga, L. F., et al. 1995, SSRv, 71, 207
Li, Q. H., Yang, L., Wu, D. J., et al. 2019, ApJ, 874, 55
Lin, R. P., Anderson, K. A., Ashford, S., et al. 1995, SSRv, 71, 125
Liu, Y., Richardson, J. D., Belcher, J. W., Kasper, J. C., & Skoug, R. M. 2006, JGRA, 111, A09108
Low, B. C. 2001, JGR, 106, 25141
Lu, Q. M., & Wang, S. 2006, JGRA, 111, A05204
Manchester, W. B., Gombosi, T. I., De Zeeuw, D. L., et al. 2005, ApJ, 622, 1225
Maneva, Y. G., Ofman, L., & Viñas, A. 2015, A&A, 578, A85
Marsch, E., Goertz, C. K., & Richter, K. 1982, JGR, 87, 5030
Maruca, B. A., Kasper, J. C., & Gary, S. P. 2012, ApJ, 748, 137
McKean, M. E., Omidi, N., & Krauss-Varban, D. 1995, JGR, 100, 3427
McKean, M. E., Omidi, N., & Krauss-Varban, D. 1996, JGR, 101, 20013
Moissard, C., Fontaine, D., & Savoini, P. 2019, JGRA, 124, 8208
Myllys, M., Kilpua, E. K. J., Lavraud, B., et al. 2016, JGRA, 121, 4378
Ofman, L., Balikhin, M., Russell, C. T., et al. 2009, JGRA, 114, A09106
Ofman, L., Gary, S. P., & ViñAs, A. 2002, JGRA, 107, 1461
Ofman, L., Viñas, A. F., & Roberts, D. A. 2017, JGRA, 122, 5839
Ogilvie, K. W., Chornay, D. J., Fritzenreiter, R. J., et al. 1995, SSRv, 71, 55
Omidi, N., Isenberg, P., Russell, C. T., et al. 2014, JGRA, 119, 1442
Omidi, N., Quest, K. B., & Winske, D. 1990, JGR, 95, 20717
Omidi, N., Thorne, R., & Bortnik, J. 2011, JGRA, 116, A09231
Podesta, J. J., & Gary, S. P. 2011, ApJ, 742, 41
Price, C. P., Swift, D. W., & Lee, L.-C. 1986, JGR, 91, 101
Quest, K. B., Forslund, D. W., Brackbill, J. U., et al. 1983, GeoRL, 10, 471
Remya, B., Tsurutani, B. T., Reddy, R. V., et al. 2014, ApJ, 793, 6
Richardson, I. G., & Cane, H. V. 2004, JGRA, 109, A09104
Richardson, I. G., & Cane, H. V. 2011, SoPh, 270, 609
Richardson, I. G., Cliver, E. W., & Cane, H. V. 2001, GeoRL, 28, 2569
Russell, C., & Blancocano, X. 2007, JASTP, 69, 1723
Russell, C. T., & Farris, M. H. 1995, AdSpR, 15, 285
Russell, C. T., Jian, L. K., Blanco-Cano, X., et al. 2009, GeoRL, 36, L03106
Russell, C. T., Mewaldt, R. A., Luhmann, J. G., et al. 2013, ApJ, 770, 38
Russell, C. T., & Mulligan, T. 2002, P&SS, 50, 527
Russell, C. T., Priest, E. R., & Lee, L. C. 1990, GMS, 58
Sanderson, T. R., Erdös, G., Balogh, A., et al. 2000, JGR, 105, 18275
Simons, D. J., Pongratz, M. B., & Gary, S. P. 1980, JGR, 85, 671
Siscoe, G., & Odstrcil, D. 2008, JGRA, 113, A00B07
Song, P., Russell, C. T., & Gary, S. P. 1994, JGR, 99, 6011
Stix, T. H. 1962, The Theory of Plasma Waves (New York: McGraw-Hill)
Tsurutani, B. T., Arballo, J. K., Mok, J., et al. 1994, GeoRL, 21, 633
Tsurutani, B. T., Gonzalez, W. D., Tang, F., Akasofu, S. I., & Smith, E. J. 1988, JGR, 93, 8519
Tsurutani, B. T., & Smith, E. J. 1984, GeoRL, 11, 331
Verscharen, D., Bourouaine, S., & Chandran, B. D. G. 2013, ApJ, 773, 163
Webb, D. F., & Howard, T. A. 2012, LRSP, 9, 3
Wilkinson, W. P. 1995, AdSpR, 15, 313
Wilson, L. B., Cattell, C. A., Kellogg, P. J., et al. 2009, JGRA, 114, A10106
Xiang, L., Wu, D. J., & Chen, L. 2018a, ApJ, 857, 108
Xiang, L., Wu, D. J., & Chen, L. 2018b, ApJ, 869, 64
Yermolaev, Y. I., Nikolaeva, N. S., Lodkina, I. G., et al. 2012, JGRA, 117, A00L07
Yoon, P. H. 2017, RvMPP, 1, 4
Zank, G. P., Hunana, P., Mostafavi, P., et al. 2015, ApJ, 814, 137
Zhao, G. Q., Feng, H. Q., Wu, D. J., et al. 2019, ApJ, 871, 175
Zurbuchen, T. H., & Richardson, I. G. 2006, SSRv, 123, 31